Spin-Peierls transition in $CuGeO_3$ and impurity-induced ordered phases in low-dimensional spin-gap systems

2002 J. Phys.: Condens. Matter 14 R195

(http://iopscience.iop.org/0953-8984/14/10/201)

INSTITUTE OF PHYSICS PUBLISHING JOURNAL OF PHYSICS: CONDENSED MATTER

J. Phys.: Condens. Matter **14** (2002) R195–R237 PII: S0953-8984(02)78680-3

TOPICAL REVIEW

Spin–Peierls transition in $CuGeO_3$ and impurity-induced ordered phases in low-dimensional spin-gap systems

K Uchinokura

Department of Advanced Materials Science, The University of Tokyo, 7-3-1 Hongo, Bunkyo-ku, Tokyo 113-8656, Japan

Received 3 January 2002
Published 28 February 2002
Online at stacks.iop.org/JPhysCM/14/R195

Abstract

The research on spin–Peierls transition and impurity-induced antiferromagnetic state(s) in $CuGeO_3$ is reviewed. In particular the recent progress of the studies of the compositional phase diagram will be discussed. The discovery of two antiferromagnetic phases in Mg-doped $CuGeO_3$ (Masuda T *et al* 1998 *Phys. Rev. Lett.* **80** 4566) opened a new aspect of this kind of research. The transition between dimerized antiferromagnetic and uniform antiferromagnetic phases is of the first order as a function of the impurity concentration. This phenomenon was studied in detail by the susceptibility, neutron diffraction, synchrotron x-ray diffraction and other methods. The existence of this transition was firmly confirmed and it was revealed that the impurity-induced phase diagram of $CuGeO_3$ is very complex. Another important problem is whether the impurity-induced ordered phase in the spin-gap system is unique to the $S = \frac{1}{2}$ spin-gap system or not. As to this problem a new Haldane-gap compound $PbNi_2V_2O_8$ was found (Uchiyama Y *et al* 1999 *Phys. Rev. Lett.* **83** 632). This compound has relatively strong inter-chain interaction. It was also found that the substitution of Mg^{2+} ions ($S = 0$) for Ni^{2+} ions ($S = 1$) induces antiferromagnetic phase in $PbNi_2V_2O_8$. From these experimental results it was shown that the occurrence of the impurity-induced ordered phase is a common feature of quasi-one-dimensional spin systems with relatively strong inter-chain interaction.

(Some figures in this article are in colour only in the electronic version)

1. Introduction

Magnetic properties of low-dimensional systems of quantum spins with antiferromagnetic (AF) interactions have attracted much attention because of their various interesting phenomena due to their quantum nature and large fluctuations, for example the spin–Peierls (SP) transition in $S = 1/2$ Heisenberg chains with spin–lattice interaction [1, 2], the appearance

of the Haldane gap in S = even integer Heisenberg chains [3] and the high-temperature superconductivity occurring in layered cuprates including CuO_2 planes [4]. In particular, AF oxides containing Cu^{2+} ions have been extensively studied since the discovery of cuprate superconductors, because the two-dimensional CuO_2 planes are responsible for the high-temperature superconductivity. At the start of our research on $CuGeO_3$ in 1992 our motivation to study the magnetic properties of low-dimensional spin systems including linear chains with Cu^{2+} ions is to compare one-dimensional Cu^{2+} based antiferromagnets with two-dimensional cuprate superconductors. This compound was suitable for magnetic studies because only Cu^{2+} ions are magnetic ($S = \frac{1}{2}$).

Studies of the SP transition have a relatively long history in theoretical and experimental research [1, 2]. Therefore the properties of the SP transition were believed to be understood well. However experimental studies were limited to organic materials [1, 2], which were difficult to grow in large single crystals and in which the doping or substitution of impurities was not easy. Therefore detailed studies of spin excitations by neutron inelastic scattering or the doping effects in inorganic SP systems had not been performed in organic SP materials.

In 1992 Hase *et al* [5] discovered a new SP compound, $CuGeO_3$, which was the first organic SP material and most probably is still the sole inorganic SP material when this review is being written. This discovery did not mean only that a new material was added to the list of SP materials but a new phase of the studies on this problem had begun with it. The reasons may be as follows.

(1) Large high-quality single crystals can be grown, which allows us to study the properties of this compound thoroughly. Especially neutron scattering can be performed to reveal spin structures and spin excitations.
(2) $CuGeO_3$ was not a good one-dimensional spin system. Moreover it cannot be described by the nearest-neighbour (nn) interaction even in the chain direction. These properties cause new phenomena even in pure $CuGeO_3$.
(3) Detailed studies on the magnetic phase, often called the M phase or incommensurate (IC) phase in strong magnetic field were performed [6] and the nature of this phase is becoming well understood. Incommensurability or discommensuration structures were experimentally confirmed, which were predicted only by the theories.
(4) Detailed studies were performed on the doping effect [7]. A completely new phenomenon, the impurity-induced AF phase, was discovered in $CuGeO_3$.

In this review general properties of $CuGeO_3$ and the SP transition will be discussed only briefly and the main part will be concerned with the impurity-induced AF state(s) in $CuGeO_3$. The new phenomenon, the problem of the spin-gap state versus the impurity-induced ordered state, will be discussed not only in $CuGeO_3$ but also in a new Haldane material $PbNi_2V_2O_8$.

2. Spin–Peierls transition in $CuGeO_3$

2.1. Structure of $CuGeO_3$

The crystal structure of $CuGeO_3$ has an orthorhombic unit cell. The space group at room temperature is *Pbmm* (*Pmma* in standard orientation) and the lattice parameters at room temperature are $a = 4.81$ Å, $b = 8.47$ Å and $c = 2.941$ Å [8]. Each Cu^{2+} ion is equivalent at room temperature. The distance between nn Cu^{2+} ions, which are situated along the c axis, is much shorter than that between the next-nearest ones along the b axis. (In a unit cell there is one Cu^{2+} ion along the c and a axes but two along the b axis.) The Cu^{2+} ions are connected via two O^{2-} ions and the angle of Cu^{2+}–O^{2-}–Cu^{2+} bonds ϕ is nearly 98°, which is rather close to 90°;

along these paths superexchange interaction may act between the $S = \frac{1}{2}$ spins on Cu^{2+} ions and the spin–spin interaction may be critical between the AF and ferromagnetic ones. According to the so-called Goodenough–Kanamori–Anderson rules [9] a $\phi = 180^\circ$ superexchange of two magnetic ions with partially filled d shells is strongly AF, while a $\phi < 90^\circ$ superexchange is ferromagnetic and much weaker. Another point is that the Ge^{4+} ions separate the CuO_2 chains. We expected that a one-dimensional AF interaction between the spins on adjacent Cu^{2+} ions in the c direction predominated over the interactions along other directions.

2.2. *Spin–Peierls transition in $CuGeO_3$*

In 1993 Hase *et al* [5] reported the detailed magnetic properties of $CuGeO_3$ and discovered the SP transition in this inorganic compound. The susceptibility versus temperature was measured along the three principal axes in a single crystal (in this case the crystal was grown by a self-flux method). The experimental result is shown in figure 1 [5]. The most striking feature was that the susceptibilities $\chi_i(T)$ in all directions ($i = a$, b and c) exponentially drop to a small constant values below 14 K. This suggested the existence of some kind of phase transition but the almost isotropic decrease of the susceptibilities rejected the possibility of the AF phase transition at 14 K. The susceptibilities above the transition temperature were almost isotropic and they have the temperature dependence characteristic of the one-dimensional AF spin system. They have a broad maximum near 56 K and slowly decrease above 56 K with increasing temperature. This broad maximum strongly indicates the existence of an AF interaction [10]. These facts suggested a possibility of one-dimensional AF chain structure and the spin–Peierls transition at 14 K. This was also supported by the change of the SP transition temperature T_{SP} with the magnetic field ($T_{SP}(H)$) shown in figure 2 [5]. According to the Hartree–Fock theory of Bulaevskii, Buzdin and Khomskii (BBK) [12] and also to the Luther–Peschel-type treatment of the spin-correlation functions of Cross [13] T_{SP} can be expressed when $\mu_B H \ll k_B T_{SP}(0)$:

$$1 - \frac{T_{SP}(H)}{T_{SP}(0)} \sim \alpha \left[\frac{\mu_B H}{k_B T_{SP}(0)} \right]^2 . \tag{2.1}$$

As shown in the inset of figure 2 the experimental result is in good agreement with equation (2.1) and the obtained value of α was $\alpha = 0.46$. This value is near the value 0.44 of Cross and not so different from the value of 0.38 of BBK. This fact also supported that the transition is an SP transition. Thus we concluded that $CuGeO_3$ has an SP transition near 14 K.

However, more strictly speaking, the temperature dependence of the susceptibilities differs distinctly from the Bonner–Fisher curve [10], which was numerically obtained for the AF Heisenberg interaction in an $S = 1/2$ chain with the Hamiltonian

$$\hat{H} = J \sum_i \boldsymbol{S}_i \cdot \boldsymbol{S}_{i+1}, \tag{2.2}$$

with $J > 0$ (AF interaction). In figure 1 the Bonner–Fisher curve is drawn with $J = 88$ K, which gives the same maximum temperature of the susceptibility as the experiment. The possible reason for the discrepancy was proposed to be the weak inter-chain coupling or the temperature dependence of the in-chain exchange interaction [5]. Another possibility is the relatively strong next-nn AF exchange interaction $J_2 = \alpha J$ in a chain. The Hamiltonian can be expressed as follows:

$$\hat{H} = J \sum_i (\boldsymbol{S}_i \cdot \boldsymbol{S}_{i+1} + \alpha \boldsymbol{S}_i \cdot \boldsymbol{S}_{i+2}). \tag{2.3}$$

The effectiveness of this interaction was first proposed by Lorenzo *et al* [14] with respect to the mechanism of phase transition but not the temperature dependence of the susceptibilities.

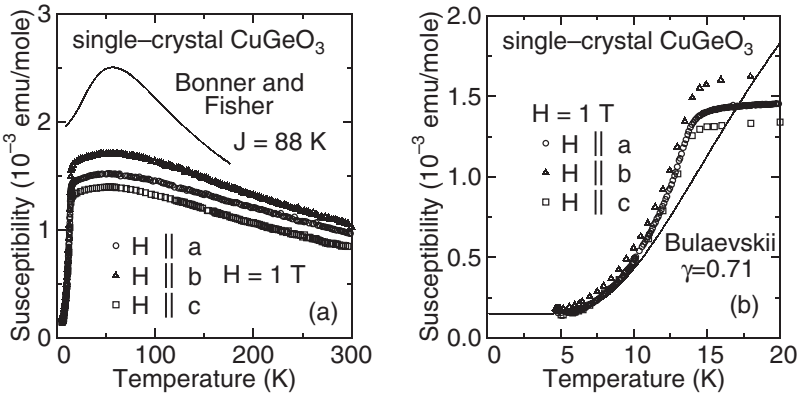

Figure 1. The magnetic susceptibility of single-crystal CuGeO measured under $H = 1$ T. (*a*) The solid curve is a theoretical one calculated by Bonner and Fisher [10] with $J = 88$ K. (*b*) The susceptibility below 20 K. The solid curve is a theoretical one calculated by Bulaevskii [11]. The value of J and the ratio between two alternating Js are 103 [$= 88(1 + 0.17)$] K and 0.71, respectively. The value of $\chi_i^{\rm orb}$ is assumed to be 1.5×10^{-4} emu mol^{-1} (reprinted from [5]).

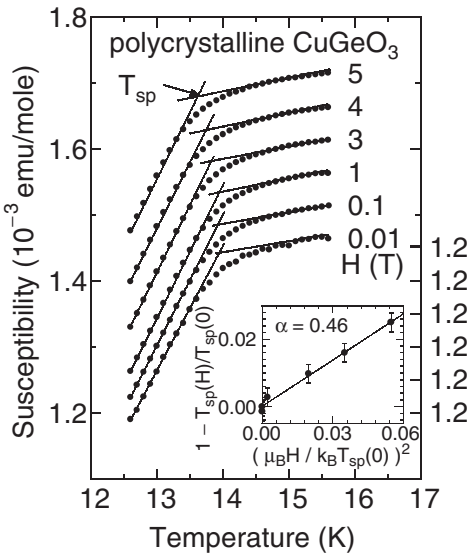

Figure 2. The magnetic susceptibility of polycrystalline $CuGeO_3$ measured near the phase transition temperature, $T_{\rm SP}(H)$, under $H = 0.01$–5 T. As is seen in this figure, each value of $T_{\rm SP}(H)$ is defined as the temperature of the intersection of two lines along each curve. The vertical position of each data point is shifted as indicated on the right-hand side of the figure. Inset: $1 - T_{\rm SP}/T_{\rm SP}(0)$ versus $(\mu_B H/k_B T_{\rm SP}(0))^2$ (reprinted from [5]).

Later Castilla *et al* [15] and Riera and Dobry [16] proposed that this kind of frustration is the main reason for the discrepancy and gave the numerical calculation to fit the experimental results of [5]. The values of $\alpha = J_2/J$ were given as 0.24 and 0.36 by [15] and [16], respectively. The former value is just below the critical one $\alpha_c = 0.2411 \pm 0.0001$ [17] for the occurrence of the double degeneracy of the ground states with energy gap and the latter is above α_c. The value of $\alpha = 0.5$ corresponds to the well known Majumdar–Ghosh model [18], in which the ground states are doubly degenerate and exactly consist of dimer states of the nn spin pairs.

At present it seems that the existence of the strong frustration (large α) is widely accepted and it is considered in the theoretical explanations of many phenomena in $CuGeO_3$. However it seems that the value of α itself has not been definitely determined.

The energy gap inherent in the SP state was observed through neutron inelastic scattering by Nishi *et al* [19]. From the dispersion relations of low-energy spin excitation they obtained the values of exchange interactions along the chain (the c direction, nn), the b and the a directions, as $J = 10.4$ meV, $J_b \sim 0.1J$ and $J_a \sim -0.01J$, respectively. Along the c (chain) and b directions the interactions are AF and along the a direction the interaction is ferromagnetic. This means that $CuGeO_3$ is not a good one-dimensional spin system, but in some sense it may be considered as a two-dimensional (or three-dimensional) spin system. This contrasts with typical organic SP materials, which were considered to be good one-dimensional spin systems. This and the large frustration in a chain add a new feature to the studies of SP materials and they cause various new phenomena, to be discussed in the later sections. The existence of a spin excitation gap was supported later by many neutron inelastic scattering experiments [20]. Among them it may be worthwhile to mention that Arai *et al* [21] observed the continuous excitation of spin as well as the gap excitation in $CuGeO_3$.

The existence of the spin gap was confirmed by other methods either directly or indirectly. Kuroe *et al* [22] have performed Raman scattering of $CuGeO_3$ at various temperatures and found the appearance of the broad feature (including some sharp structures) as well as several new phonon peaks below T_{SP} in $CuGeO_3$. The broad feature ranges from 30 to $\sim$230 cm^{-1}. Supposing that this spectrum is due to the second-order Raman scattering of the spin excitation observed by Nishi *et al* [19], they calculated the two-magnetic-excitation density of states $D(\omega/2)$ based on the values of Js obtained by Nishi *et al* (to fit the experimental data Js were slightly different from those of Nishi *et al*). The overall feature of $D(\omega/2)$ is very similar to the obtained spectra but at the lowest-energy region the Raman spectrum has an asymmetric peak at $\sim$30 cm^{-1}, whereas $D(\omega/2)$ does not have a peak. This part of the spectrum is shown in figure 4; it is taken from the more recent [23] to show data with better S/N and resolution. This fact suggests that this spectrum is of magnetic origin. The temperature dependence of the energy $\hbar\omega_0(T)$ of the 30 cm^{-1} peak was obtained (see figure 5 of [22]) and it was very close to twice the gap energy $2\Delta(T)$ obtained by the neutron inelastic scattering by Nishi *et al* [19], but $\hbar\omega_0(T)$ was slightly less than $2\Delta(T)$. Kuroe *et al* [22, 23] concluded that this broad feature (except for the 184 cm^{-1} phonon peak) is due to the two-magnetic-excitation spectrum, and the formation of a peak at 30 cm^{-1} and the energy shift of $2\Delta(T)$ is due to the formation of the bound state with two gap-energy excitations.

Another observation of the spin gap was made earlier through the nuclear quadrupole resonance (NQR) study by Kikuchi *et al* [24]. The NQR signals of ^{63}Cu and ^{65}Cu were observed under zero magnetic field. These signals persisted down to 1.3 K with neither line splitting nor broadening due to internal magnetic field. This indicated that there is no long-range order of Cu spins. The ^{63}Cu nuclear spin–lattice relaxation rate $^{63}(1/T_1)$ rapidly drops below 15 K, which clearly demonstrated an opening of the energy gap in the spin excitation spectrum (see figure 5 [24]).

Another inherent property of the SP system is the existence of dimerization of the lattice. This was not found easily. Many neutron and x-ray diffraction experiments failed to observe it. Therefore some researchers doubted the validity of the SP transition as the mechanism of the phase transition in $CuGeO_3$. However, more than a year after the discovery of the SP transition in $CuGeO_3$ the dimerization of the lattice was finally found almost at the same time by electron, x-ray and neutron diffraction. Kamimura *et al* [25] observed superlattice reflections due to lattice dimerization by electron diffraction; the satellite reflections were observed by means of neutron diffraction by Hirota *et al* [26] and by Pouget *et al* [27] and by means of x-ray

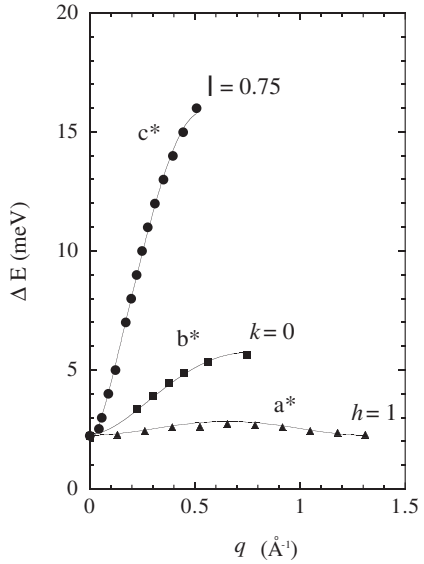

Figure 3. The dispersion relations of the magnetic excitons in $CuGeO_3$ along each principal axis at $T = 4$ K. The solid curves indicate resultant curve fittings using the Heisenberg AF spin-wave formula. (0, 1, 0.5) is the zone centre; $q = 0$ (reprinted from [19]).

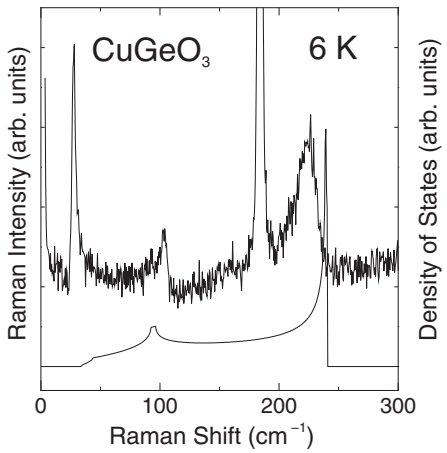

Figure 4. Raman spectrum at 6 K in pure $CuGeO_3$ below 300 cm^{-1}. A solid curve denotes the two-magnetic-excitation density of states $D(\omega/2)$ (reprinted from [23]).

diffraction [27]. The reason for the difficulty of finding the dimerization turned out to be that the dimerization was not a simple one and the satellite peaks do not exist along the c^* direction, where the earlier studies searched. Among them Hirota *et al* observed the superlattice peak at $h/2\ k\ l/2$ (h, l odd, k even) in addition to those with k odd, which were found in [25,27]. They determined the lattice structure below T_{SP} and concluded that the highest possible space group for the doubled cell is *Bbcm* (*Cmca* in standard orientation). The temperature dependences of the superlattice reflections at (1/2 5 1/2) and (1/2 6 1/2) are shown in figure 6 [26]. They also determined the displacements of the atomic positions as shown in figure 7 [26].

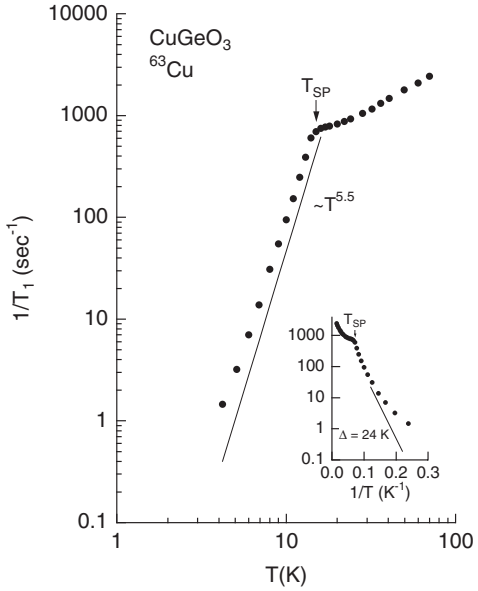

Figure 5. Temperature dependence of $^{63}(1/T_1)$ in $CuGeO_3$ plotted in a logarithmic scale. The solid line represents the power law $1/T_1$ versus $1/T$ plot of $^{63}(1/T_1)$. The slope of the straight line in the inset corresponds to the energy gap $\Delta = 24$ K (at $T = 0$ K) of [5] (reprinted from [24]).

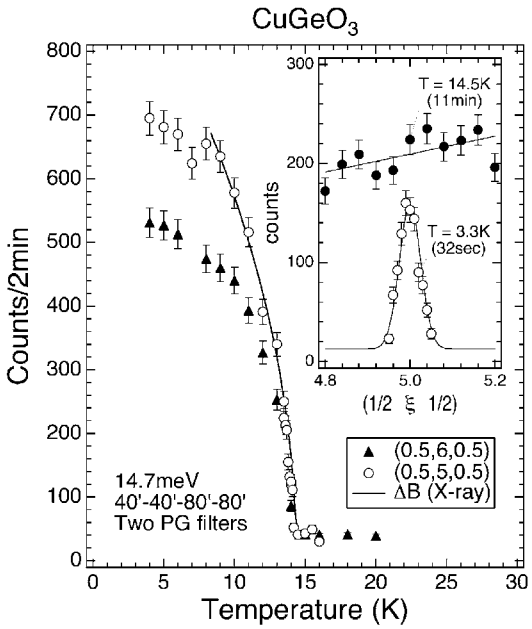

Figure 6. The temperature dependence of the superlattice reflections at (1/2 5 1/2) and (1/2 6 1/2) on heating. Peak profiles of the (1/2 5 1/2) reflection at 3.3 and 14.5 K (T_{SP}= 14.2 K) are shown in the inset (reprinted from [26]).

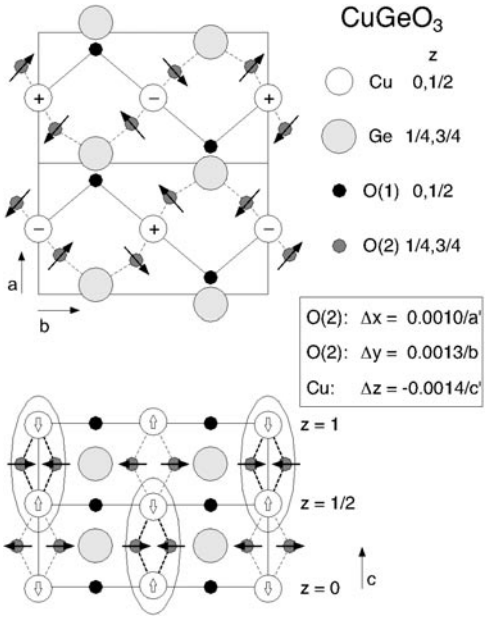

Figure 7. Schematic representation of the low-temperature structure for $CuGeO_3$ in the SP state. The rectangles show the unit cell for the high-temperature structure. The cell becomes doubled in the a and c directions below T_{SP}. Arrows and signs indicate the directions of displacements. For clarity, atomic displacements are drawn ten times larger than reality (reprinted from [26]).

The change of the structure below T_{SP} was also observed by optical methods: Raman scattering [22] and infrared spectroscopy [28, 29].

The magnetization saturation of $CuGeO_3$ was observed by Nojiri *et al* [30] using ultrahigh magnetic fields up to 500 T. Faraday rotation through a single crystal was measured. As shown in figure 8 [30] the magnetization (Faraday rotation angle) curve shows a nonlinear increase with the magnetic field, which is a typical behaviour of a one-dimensional quantum spin system. The magnetization saturation was distinctly observed at 253 T. From this the exchange parameter was obtained as 183 K or 15.8 meV, which is substantially larger than the value $K = 10.4$ meV of Nishi *et al* [19].

3. Incommensurate phase in $CuGeO_3$

One of the characteristic properties related to the SP transition is the existence of an IC phase in high magnetic field. Experimentally in the organic SP materials the phase transition from the SP phase (i.e. dimerized or commensurate phase) to a magnetic phase was observed long ago [33–35]. Many theories were proposed on this phase and this magnetic phase is known to have an IC structure with respect to both the lattice displacement and the spin order [36–39]. However the direct experimental observation of the IC structure had not been made in organic SP materials until the discovery of the SP transition in $CuGeO_3$.

Now the situation has drastically changed and a number of phenomena concerned with this commensurate-to-incommensurate (C–IC) transition are understood now.

Just after the work of [5] the author's group found the C–IC transition by measuring the magnetization versus magnetic field by using pulsed magnetic field up to 25 T [6]. Below 13.4 K a characteristic nonlinearity of the magnetization was observed, which corresponds to

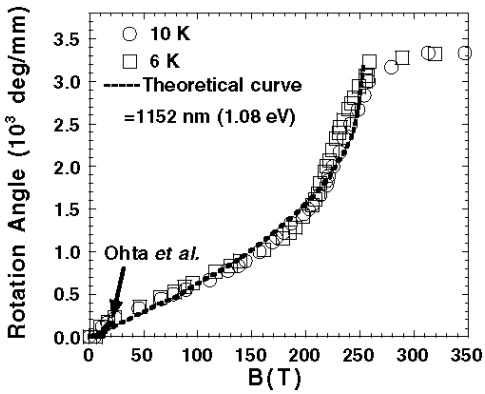

Figure 8. Plot of Faraday rotation angle against the magnetic field. The wavelength is 1152 nm from a He–Ne laser. The dashed curve is the theoretical curve for an $S = 1/2$ uniform Heisenberg AF chain at $T = 0$ K from [10, 31]. The thick curve shows the magnetization data from [32] (reprinted from [30]).

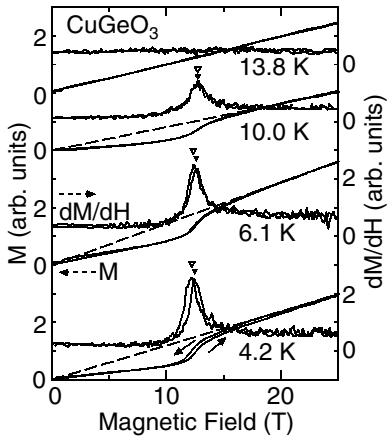

Figure 9. The magnetic-field dependence of M and $\mathrm{d}M/\mathrm{d}H$ of polycrystalline $CuGeO_3$. Closed and open triangles denote the peak positions of $\mathrm{d}M/\mathrm{d}H$ measured in increasing and decreasing fields, respectively. Solid arrows represent the directions of the scans of the field. Dashed lines indicate the extrapolation of M from the high-field region to $H = 0$ (reprinted from [6]).

the C–IC transition. As shown in figure 9 [6], this transition was hysteretic below 10 K, which means that the transition is first order. Above 10 K, no hysteresis was observed and the transition seems to be second order there. The critical field of the transition was 12–13 T. Figure 10 shows the phase diagram of $CuGeO_3$, which is drawn as the relation between $gH/2T_{SP}(0)$ and $T/T_{SP}(0)$ [6]. The magnetic phase diagram of $CuGeO_3$ agrees qualitatively with both experimental results of typical organic SP materials [33–35] and a theoretical one [36]. This indicates the universal nature of the phase diagram of SP systems, either organic or inorganic.

In figure 10 [6] the phase boundary between the IC (M) and uniform (U) phases was not observed. The first observation of this boundary in $CuGeO_3$ was made by Hamamoto *et al* [40] by using ac susceptibility measurement up to 20 T in a superconducting magnet and a hybrid magnet.

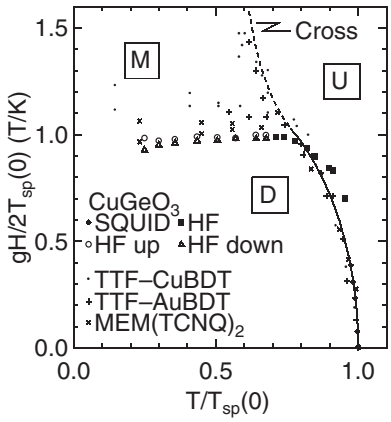

Figure 10. The magnetic phase diagram of $CuGeO_3$. Open circles, open triangles and closed squares represent the critical fields determined from the magnetizations in the high magnetic fields up to 25 T, and closed diamonds spin–Peierls transition temperatures measured by a SQUID magnetometer. This figure includes the data of typical organic SP materials. Solid and dashed curves are theoretical ones. U, D and M denote dimerized (SP), uniform and magnetic (incommensurate) phases, respectively. References: TTF-CuBDT from [33], TTF-AuBDT from [34], $MEM(TCNQ)_2$ from [35] and theoretical curves from [13] (reprinted from [6]).

The hysteretic behaviour of the C–IC transition was more clearly observed by the high-field electron spin resonance (ESR) measurement. As shown in figure 2 of [32] the resonances from the IC and the dimerized phases coexist near the critical field [32], which confirms that the transition is first order.

In 1995 Kiryukhin *et al* [41] reported the direct observation of the superstructure due to the IC structure in organic charge transfer salt TTF-CuBDT by using high-resolution x-ray diffraction in magnetic fields up to 12.5 T.

Almost at the same time Kiryukhin *et al* [42–44] observed the IC lattice modulation in $CuGeO_3$ by the same method. As shown in figure 11 [44] they observed the superlattice diffraction with the IC wavenumbers. In the scans through the (3.5, 1, 2.5) reflection in the spin–chain direction below 12 T only a single diffraction peak corresponding to the lattice dimerization was observed. In higher magnetic fields the reflection peak is split. The wavenumber vectors are incommensurate with the reciprocal lattice of the dimerized phase and depend on the magnetic field. Coexistence of the commensurate and incommensurate peaks was observed in a narrow field range near the critical field, which shows the transition is first order. Also a weak third-harmonic reflection was clearly visible (see figure 3 of [44]). Thus the discommensurate structure or soliton nature of the IC lattice displacement near the critical field was directly observed and discussed in comparison with theories.

The x-ray diffraction detects only the lattice displacements. The IC spin structure was very recently studied by nuclear magnetic resonance (NMR) [45, 46] and detailed neutron diffraction [47].

Horvatić *et al* [46] obtained the soliton lattice profile in the IC phase of $CuGeO_3$ by using NMR imaging. They measured the evolution of ^{65}Cu NMR line shapes when H is varied from H_c (critical field) to $\simeq 2H_c$ (see figure 12 [46]). Up to H_c (=13 T) only a narrow symmetric line was seen, corresponding to the homogeneous zero-spin polarization in the dimerized phase. Just above H_c the line was strongly broadened and a wide distribution due to solitons appeared. With increasing H, the broadened zero-spin polarization was rapidly suppressed, reflecting

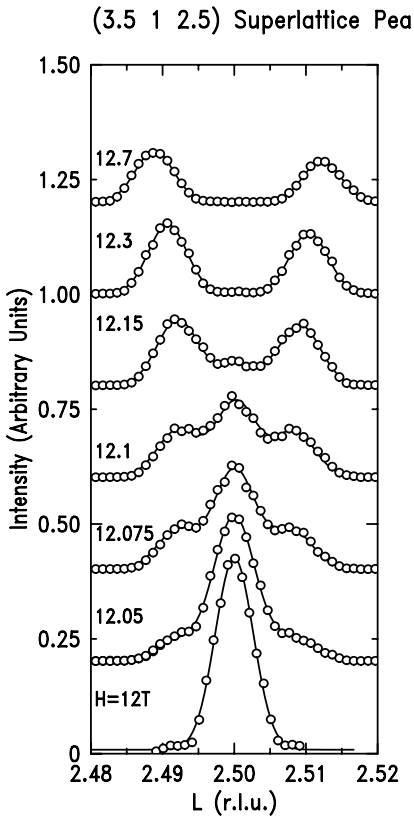

Figure 11. Scans through the (3.5, 1, 2.5) (x-ray) superlattice reflection of pure $CuGeO_3$ at $T = 4$ K for different magnetic fields (reprinted from [44]).

the disappearance of the nearly dimerized regions and the approach towards a plane-wave-like region. The NMR line shapes were fitted to the theoretically expected profile of the soliton lattice (see figure 13 [46]). In the continuum approximation, the IC phase is described by a phase variable which satisfies a sine–Gordon equation [37, 38, 48]. The solutions were given in terms of the Jacobi elliptic functions: sn for a lattice distortion, dn and cn for the average and staggered components of the spin polarization. The total spin polarization was written as [48]

$$\langle S_z(i)\rangle = \frac{W}{2}\left[\frac{1}{R}\mathrm{dn}[ic/(k\xi), k] + (-1)^i \mathrm{cn}[ic/(k\xi), k]\right], \tag{3.1}$$

where i counts the position of the spins in the chain along the c direction and for other notations[1]. The results are shown in figure 13 [46]. Using the fact that the soliton lattice period L contains two solitons with an $S = 1/2$ spin [37, 38, 49] and therefore $\langle \bar{S}_z\rangle L = 1$, they found experimentally that $1/L = \langle \bar{S}_z\rangle$ is proportional to $1/\ln[8/(H/H_c - 1)]$. This was predicted within the mean-field theory [49] and was also found experimentally in an organic spin–Peierls compound [2]. The correlation length was also obtained using the relation $\xi = L/4kK(k)$,

[1] Notations in equation (3.1): ξ is the correlation length defined by the corresponding sine–Gordon equation, R is the ratio of amplitudes of the staggered and average component of spin polarization, k is the modulus of elliptic functions and $W/2$ is the amplitude of the staggered component.

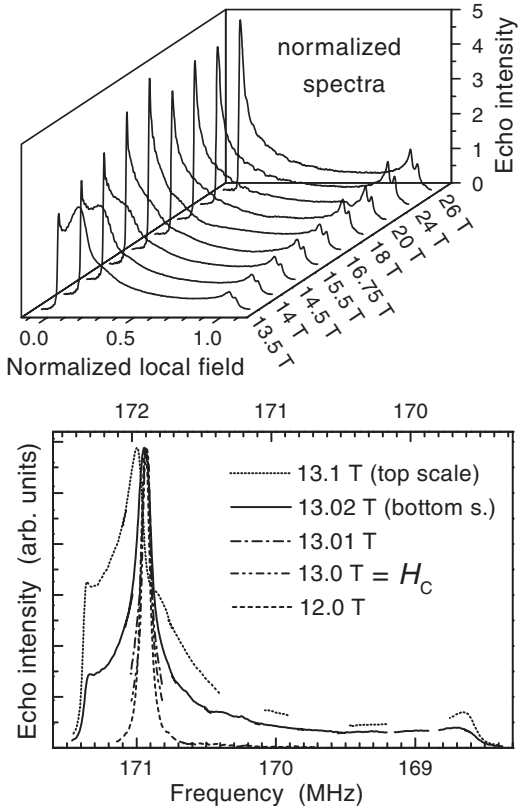

Figure 12. Magnetic field dependence of ^{65}Cu NMR line shape in a $CuGeO_3$ single crystal at 4 K for $h = (H - H_c)/H_c$ varying in the range 0.0015–1. In the bottom panel, the spectra have been recorded by sweeping the frequency. The frequency scales of these spectra are mutually shifted by $\Delta\nu = {}^{65}\gamma\,\Delta H$ in order to compensate for the variations of the magnetic field and for the 12–13.01 T spectra the corresponding scales are *not* shown. In the top panel the spectra correspond to field sweeps (reprinted from [46]).

where $K(k)$ is the complete elliptic integral of the first kind. The value of the ratio R between the amplitudes of the staggered and averaged components was definitely several times smaller than that predicted by the theories [37, 38, 50].

By the neutron diffraction studies Rønnow *et al* [47] observed directly a long-range magnetic soliton structure (see figure 14 [47]). The averaged part of the magnetic structure should give rise to even harmonics around integer positions in reciprocal space, as indicated in equation (3.1). The second-order harmonics were clearly found near the (0, 0, 1) Bragg reflection, as shown in the inset of figure 14 [47].

Recently Takehana *et al* [51] have found a very interesting phenomenon in the IC phase. As has already been discussed, in the SP phase some of the zone-edge phonon modes in the uniform phase become Raman or infrared active and these 'folded modes' were observed [22, 28, 29]. Among them 107 cm^{-1} (A_g) and 369 cm^{-1} (A_g) modes were studied also in the IC phase [52]. Splitting of the modes was not reported in these or any other modes (except for the 98 cm^{-1} mode). In contrast to these facts, as shown in[2] figure 15, Takehana *et al* [51] found the splitting

[2] Due to the symmetry of the FP mode (B_{3u}) it has the polarization characteristic $\boldsymbol{E} \parallel a$. For this mode to be observed, the sample with cleaved *bc* surface must be tilted in relation to the incident light (see [51] for details).

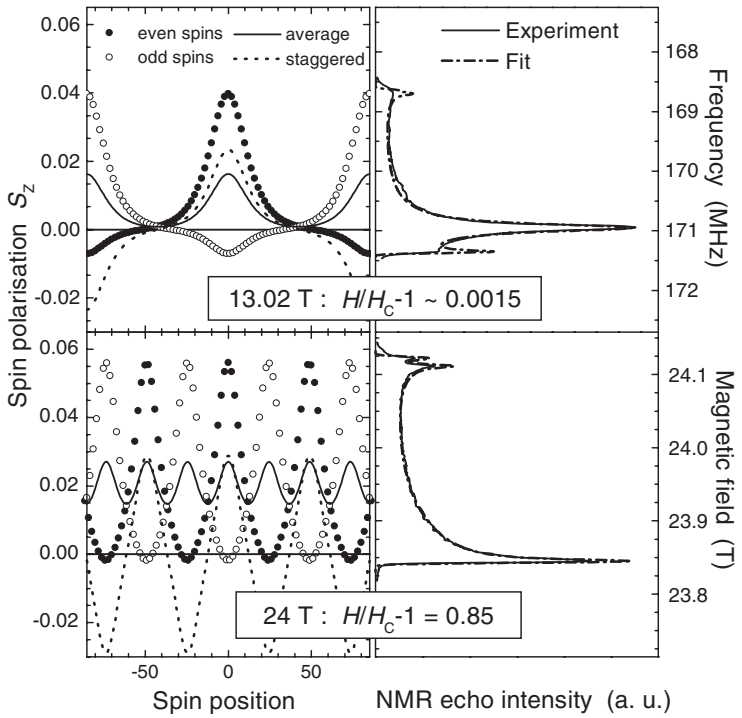

Figure 13. Real space reconstruction of the spin polarization profile (left) and the corresponding fit to Jacobi elliptic functions superimposed on experimental spectra (right). The top left panel shows one period of the soliton lattice taken at a field only 0.15% above H_c, with soliton peaks well separated by 'dimerized' regions. High above H_c (bottom panels) these regions disappear and solitons strongly overlap making the profile more sinusoidal (reprinted from [46]).

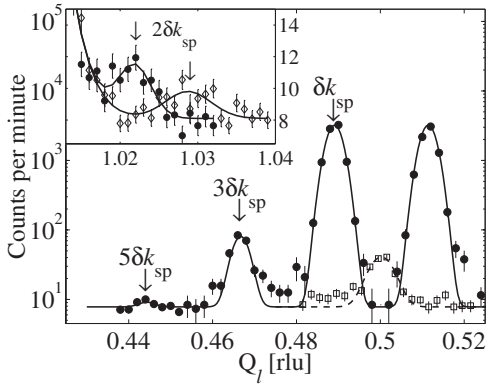

Figure 14. Scans along [00ℓ] through (1/2, 1, 1/2) at 1.6 K and 0 T (squares), and 13 T (filled circles). The resolution-limited peaks were fitted to Gaussian line shapes. The higher harmonics $n\delta k_{SP}$ are marked by arrows. The inset shows scans through (0, 0, $1+2\delta k_{SP}$) at 13 T (filled circles) and 14.5 T (diamonds) (reprinted from [47]).

of the 98 cm^{-1} (B_{3u}) mode (this mode was designated as the FP mode) into two modes (FP_L and FP_U modes) in the IC phase and the coexistence of the FP mode and the FP_L and FP_U modes near H_c. The peak positions of FP, FP_L and FP_U modes are plotted in figure 16 [51].

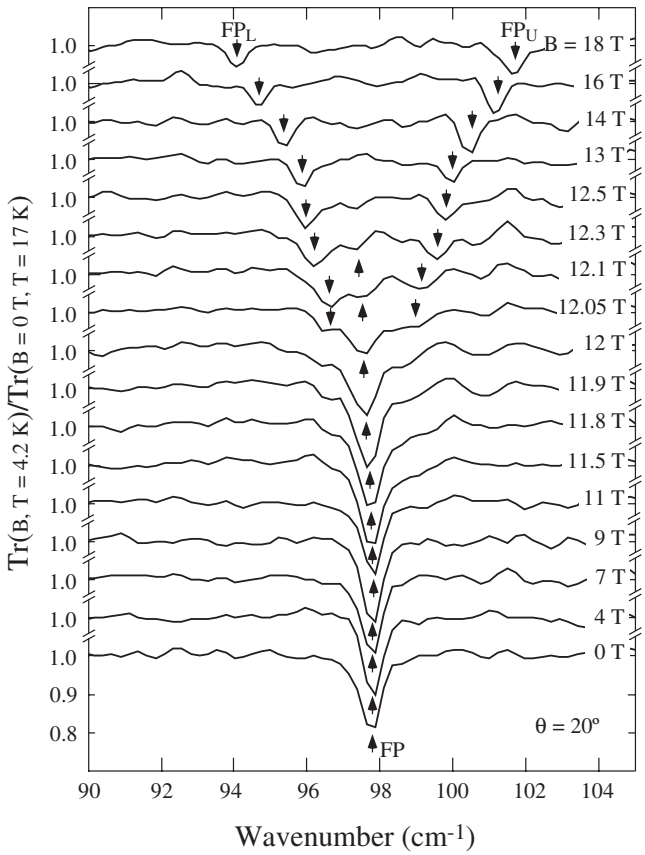

Figure 15. Field dependence of the absorption at 98 cm^{-1} at 4.2 K, when the sample is rotated by 20°. Satellite peaks appear on both sides of the absorption at 98 cm^{-1} in the IC phase, while the main peak weakens and disappears around the critical field (reprinted from [51]).

This phenomenon was explained as follows. The 98 cm^{-1} phonon is a spin–phonon coupled mode. Here we should recall that the soft phonon related to the SP transition has never been observed and now it is believed that there is no soft mode in $CuGeO_3$. However, because the SP transition occurs in $CuGeO_3$, some of the phonon modes must be strongly coupled with spin. Such a mode may be called a spin–phonon coupled mode. In the IC phase a folded mode with a wavenumber $\pm(\boldsymbol{q}_{SP} - \Delta\boldsymbol{q})$ can be observed by infrared or Raman experiment instead of the mode with $\boldsymbol{q}_{SP}$, which may be Raman or infrared active in the dimerized phase. Here $\boldsymbol{q}_{SP}$ is the wavenumber vector which represents the distortion in the SP phase and $\pm(\boldsymbol{q}_{SP} - \Delta\boldsymbol{q})$ represent that of the IC phase. If a folded mode is not coupled with spin (or only weakly coupled with spin), there is no (or very weak) coupling between the $\pm(\boldsymbol{q}_{SP} - \Delta\boldsymbol{q})$ modes and only one Raman or absorption peak is observed, i.e. no splitting in the IC phase. A spin–phonon coupled mode has a component of the lattice vibration as well as the oscillation of the spin component. As was observed in the NMR experiment [46] and neutron diffraction experiment [47] in the IC phase the static distortion has the spin component of $2\Delta\boldsymbol{q}$, which causes the coupling between the spin components of the $\pm(\boldsymbol{q}_{SP} - \Delta\boldsymbol{q})$ modes. Therefore some of the folded mode (spin–phonon coupled mode) can be split into two peaks. The authors of [51] claimed that the FP mode is just this kind of spin–phonon coupled mode and

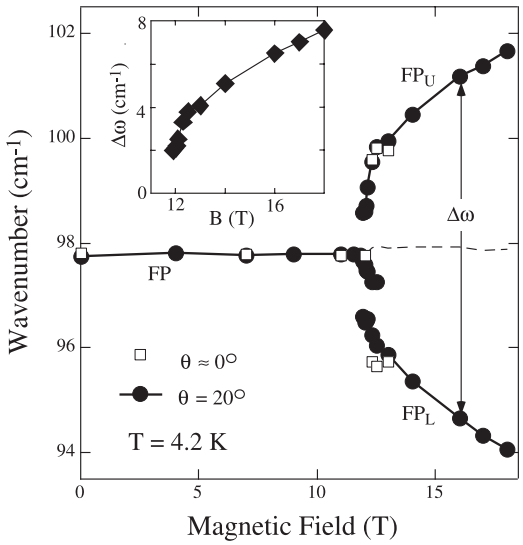

Figure 16. Field dependence of the peak positions of the absorption at 98 cm^{-1} and its satellites at 4.2 K, when the sample is rotated by a few degrees (open squares) and 20° (closed circles). The dashed curve indicates the field dependence of the average energy of the satellites. The inset shows the field dependence of the energy separation between these satellites, $\Delta\omega$ (reprinted from [51]).

that the splitting into FP_L and FP_U modes is another proof of the existence of static $2\Delta\boldsymbol{q}$ spin modulation in the IC phase. They also showed that $\Delta\omega/H_c$ is scaled with $\Delta q/H_c$ and can be fitted with $1/\ln[8/(H/H_c-1)]$ (see figure 10 of [51]). Here $\Delta\omega$ is the splitting energy between FP_L and FP_U. This fact is consistent with the model that the FP mode is a spin–phonon coupled mode. In the soliton model the average magnetization is caused by the induced $S = 1/2$ spins at the domain boundaries, i.e. two of the $S = 1/2$ spins per L in a chain. This causes the splitting of the FP mode, which is naturally proportional to $\Delta q = 2\pi/L$ [51]. This experiment is the first explicit observation of a spin–phonon coupled mode, which will play an important role to understand the SP transition in $CuGeO_3$.

The IC phase and magnetic phase diagram of pure $CuGeO_3$ have been studied by various methods, for example by magnetostriction and thermal expansion in [53, 54], by far-infrared spectroscopy in [55], by ESR and magnetization in [56,57] and by thermal conductivity in [58].

4. Impurity-induced antiferromagnetic phase in $CuGeO_3$

4.1. Antiferromagnetic phase

Just after the discovery of the SP transition in pure $CuGeO_3$, the effect of the substitution of nonmagnetic Zn^{2+} ions ($S = 0$) for Cu^{2+} ions ($S = 1/2$) was investigated by Hase *et al* [7]. They observed that (a) the SP transition temperature decreases with increasing Zn concentration x ($Cu_{1-x}Zn_xGeO_3$), (b) the magnitude of the susceptibility increases with x and most prominently (c) a new phase appears below T_{SP} (see figure 17 [7]). The phase was first assigned to a spin-glass state [7] but it turned out later that the correct phase is AF phase [59–61]. Figure 18 [60] shows that the susceptibility is anisotropic and the spin-flop transition is observed when the magnetic field is along the c axis in the single-crystal $Cu_{1-x}Zn_xGeO_3$ with $x \sim 0.04$. These facts exhibit that the transition is the AF one

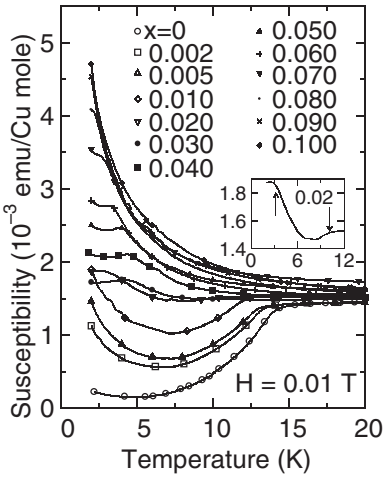

Figure 17. The magnetic susceptibilities of polycrystalline $Cu_{1-x}Zn_xGeO_3$ below 20 K measured under $H = 0.01$ T in the field-cooling process. The data were measured at an interval of 0.2 K in general. Inset: the susceptibility of the sample with $x = 0.02$. Arrows indicate the positions of the phase transitions (reprinted from [7]).

with the easy axis along the c axis in this case [60]. Moreover neutron diffraction [61] of $Cu_{0.966}Zn_{0.034}GeO_3$ shows magnetic Bragg reflections (see figure 19 [61]) below T_N and the spin configuration was determined: the nn spins align antiparallel and parallel to each other along the b axis and along the a axis, respectively. This configuration is consistent with the signs of the exchange interactions obtained in pure $CuGeO_3$ [19].

Now it has been established that the AF long-range order (AFLRO) occurs in $Cu_{1-x}M_xGeO_3$ (M = Zn [7, 59–62], Ni [59, 62–64], Mn [59]) and $CuGe_{1-y}Si_yO_3$ [68]. The easy axis is along the c axis except for Ni doping, where it is nearly along the a axis [62–64].

The important point is that this phase is not the conventional AF phase but it has very special features.

One of these is the coexistence of the AFLRO and the LRO of the dimerization due to the SP transition in the low-concentration region. In the first report of the impurity effect [7] it has already been reported that in $Cu_{1-x}Zn_xGeO_3$ the new phase (AF phase) exists below the SP transition temperature (T_{SP}) at $x < 0.02$, while at higher x only the AF transition is observed. In the region of $x < 0.02$ the magnetization versus magnetic field relation measured by using pulse and static magnetic fields [65–67] showed distinctly the transition to the IC phase (see figure 20 [65]) very similar to that of pure $CuGeO_3$. This indicates clearly that there exists a spin-gap excitation in the AF phase (in the concentration and temperature regions of AF AFLRO) and the spin gap is closed by the applied magnetic field. This immediately means that there exists dimerization which is coupled with the spin gap. Therefore in this region of the AF phase spin-wave excitation, which is inherent to the AF phase, and the spin-gap excitation, which is coupled with the dimerization, coexist. The coexistence was confirmed by neutron diffraction in $CuGe_{1-y}Si_yO_3$ [69], $Cu_{1-x}Zn_xGeO_3$ [70, 71] and $Cu_{1-x}Ni_xGeO_3$ [72]. The neutron diffraction intensity of the superlattice Bragg reflection due to dimerization decreases when the magnetic Bragg peak appears below the AF transition temperature (T_N).

Fukuyama *et al* [73], applying the phase Hamiltonian method, obtained the state with the coexisting order parameters at $T = 0$ K, and explained the $CuGe_{1-y}Si_yO_3$ experiment of [69]. According to their theory local strain around the doped Si reduces the spin–Peierls

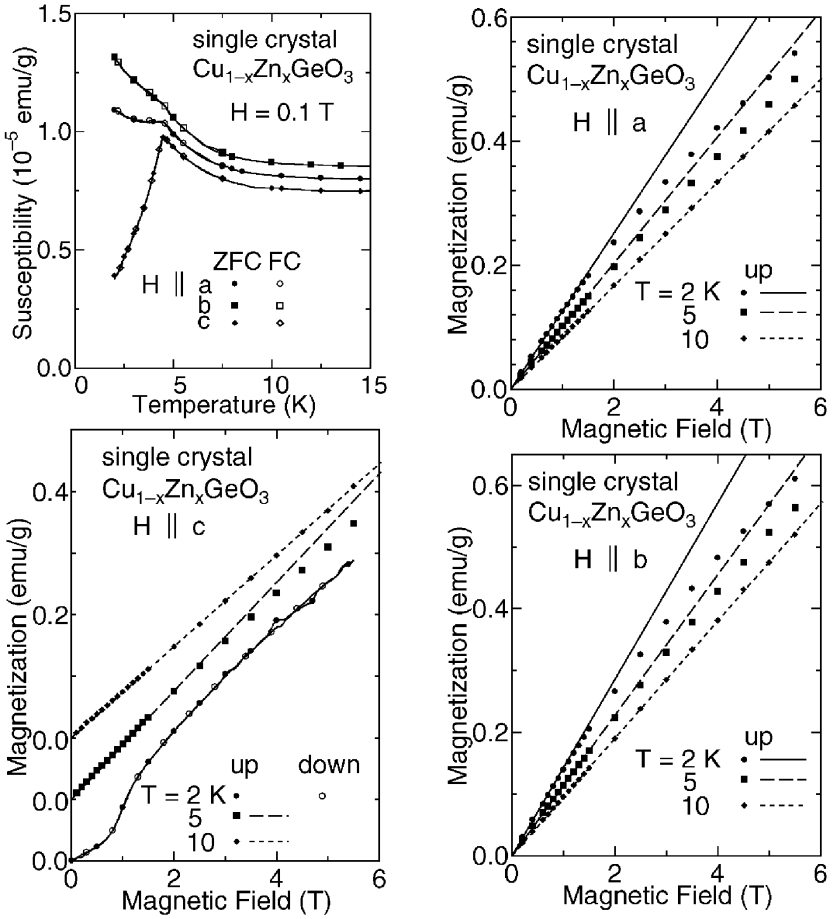

Figure 18. Upper left panel: temperature dependence of the magnetic susceptibility in the zero-field-cooling (ZFC) and field-cooling (FC) processes. The magnetic field dependences of the magnetization when the magnetic field is (upper right panel) along the c axis and (lower panels) along the a and b axes of $Cu_{1-x}Zn_xGeO_3$ with $x \sim 0.04$ (reprinted from [60]).

lattice dimerization and accordingly the AFLRO appears; i.e. both the lattice order parameter and the spin order parameter can coexist, while they have a large spatial variation. The ordered moments (lattice dimerization) become maximum (minimum) around the doping centre, and the spatial envelopes are described by the elliptic functions [73] (see figure 21 [73]).

Kojima *et al* [74] reported muon spin relaxation measurement of the doped SP system $(Cu_{1-x}Zn_x)(Ge_{1-y}Si_y)O_3$ and confirmed the presence of AF order in this series of compounds. The muon-spin precession is accompanied by a relaxation signal indicating a large spatial inhomogeneity of the ordered moment size. Assuming an exponential decay of the moment size away from the doping centres, they estimated a decay length of $\xi \sim 10$ lattice size along the chain.

Thus in the low-x region the AF phase may be explained as the AF state, which also has the dimerization, in $Cu_{1-x}Zn_xGeO_3$, $Cu_{1-x}Ni_xGeO_3$ and $CuGe_{1-y}Si_yO_3$. The AF phase in the high-x region, on the other hand, was somewhat controversial. The neutron diffraction experiments by Sasago *et al* [70] and Martin *et al* [71] showed that the dimerization is

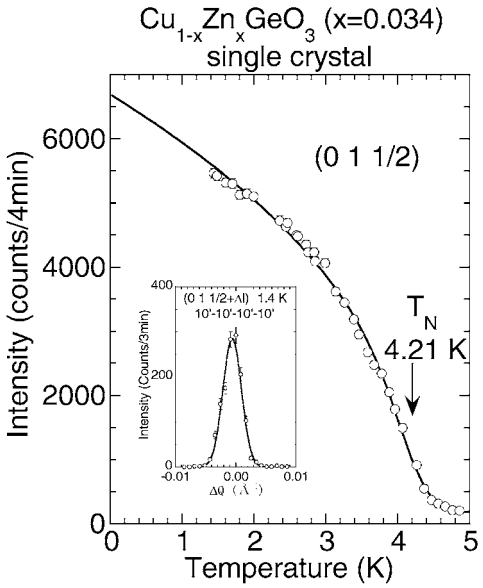

Figure 19. The temperature dependence of the intensity of the magnetic Bragg peak at (0 1 1/2) in single-crystal $Cu_{0.966}Zn_{0.034}GeO_3$. Inset: a profile of the (0 1 1/2) peak at 1.4 K is shown. The solid curve represents a Gaussian curve with the width equal to the resolution width (reprinted from [61]).

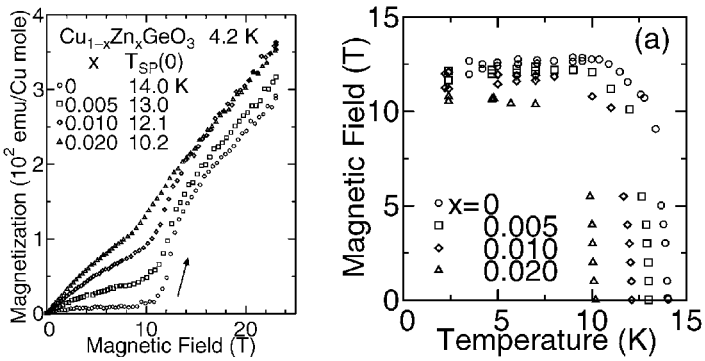

Figure 20. Left panel: magnetization versus magnetic field relation of $Cu_{1-x}Zn_xGeO_3$ at 4.2 K. Right panel: the magnetic phase diagrams of $Cu_{1-x}Zn_xGeO_3$ (reprinted from [65]).

still observed above an x value where the decrease of the magnetization due to spin–Peierls transition ceases to be observed in $Cu_{1-x}Zn_xGeO_3$. Such a phenomenon had not been observed in $CuGe_{1-y}Si_yO_3$. The change of the AF phase from the low-x to the high-x region has not been fully understood.

The recent report of Masuda *et al* [75] showed a new feature of impurity-induced AF phases and the relation between the dimerization and AFLRO. According to this there are two kinds of AF phase in $Cu_{1-x}Mg_xGeO_3$ as a function of Mg concentration x. One of them is the dimerized antiferromagnetic (DAF) phase, which has the dimerization of the lattice and the AFLRO at the same time. This is the same state as already discussed. The other is the uniform antiferromagnetic (UAF) phase, in which, it is claimed, only the AFLRO exists and

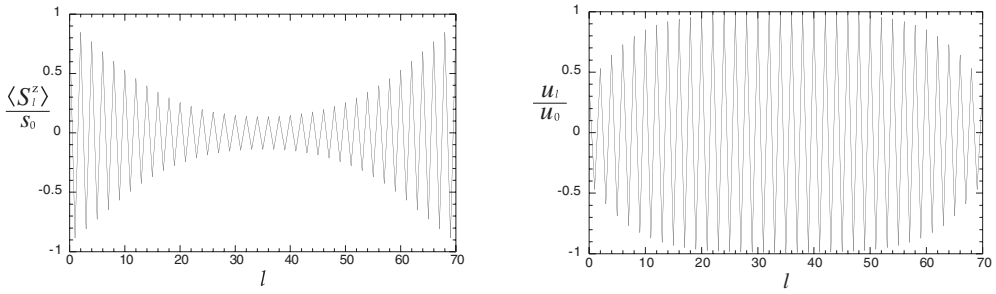

Figure 21. The spatial variation of (left panel) the magnetic staggered moment $\langle S_l^z \rangle / s_0$ and (right panel) the lattice distortion u_l/u_0 in the case of $L_0/a = 70$ and $u_{\rm imp}/u_0 = 0.4$. Here a is the lattice constant along the chain (reprinted from [73]).

the dimerization is absent (or the dimerization has only short-range order). Between these phases there is a first-order phase transition. The critical concentration x_c was reported to be near 0.023 [75].

Another important problem is whether the AF phase continues to exist up to zero impurity concentration or not. Manabe *et al* [76] studied this problem in $Cu_{1-x}Zn_xGeO_3$. The experimental results show that there is no critical concentration for the occurrence of the AF phase transition.

A more important aspect of this problem is whether the impurity-induced ordered phase(s) in the spin-gap systems is (are) unique to the $S = 1/2$ spin-gap system or not. There had been no reports of the observation of an impurity-induced AF state in another typical spin-gap system, the $S = 1$ one-dimensional spin-gap system, which has a Haldane gap [3]. Therefore to solve this problem it was necessary to find a compound with a Haldane-gap ground state. We have found that $PbNi_2V_2O_8$ has a Haldane-gap state as the ground state. It was also found that it has relatively strong inter-chain interaction. We found the impurity-induced AF phase in this material [77].

In the following the recent experimental works on impurity-induced AF phases in an SP system, $CuGeO_3$ and a Haldane-gap system, $PbNi_2V_2O_8$ will be reviewed.

4.2. Existence of two kinds of antiferromagnetic phase

Here I shall discuss a new phenomenon: that there exist two distinct AF phases and that there occurs a first-order phase transition between them as a function of the concentration of the impurities, which were found by Masuda *et al* [75]. The reason for using $Cu_{1-x}Mg_xGeO_3$ instead of $Cu_{1-x}Zn_xGeO_3$, which had been mainly used for the substitution effect of $S = 0$ impurities, was the following: prior to this it was found that the homogeneity of the impurities in the single crystals grown by the FZ method is much better in $Cu_{1-x}Mg_xGeO_3$ than in $Cu_{1-x}Zn_xGeO_3$ except for the lightly doped region. This is in contrast to the fact that in the solid-state reaction method Mg cannot be properly doped in $CuGeO_3$. Therefore it turned out that $Cu_{1-x}Mg_xGeO_3$ is more appropriate than $Cu_{1-x}Zn_xGeO_3$ for studying the detailed temperature–impurity concentration phase diagram, particularly in the heavily doped region.

The susceptibilities along the c axis, $\chi_c(T)$, of typical Mg-doped $CuGeO_3$ samples are shown in figure 22(a) [75]. The details near $T_{\rm N}$ are shown in figures 22(b)–(e) [75]. A single sharp transition is observed below and above $x = 0.023$ in figures 22(b), (d) and (e). Broadening of the cusp is observed at $x = 0.023$, as shown in figure 22(c). This behaviour suggests the existence of two transition temperatures $T_{\rm N1}$ and $T_{\rm N2}$, which is caused by the

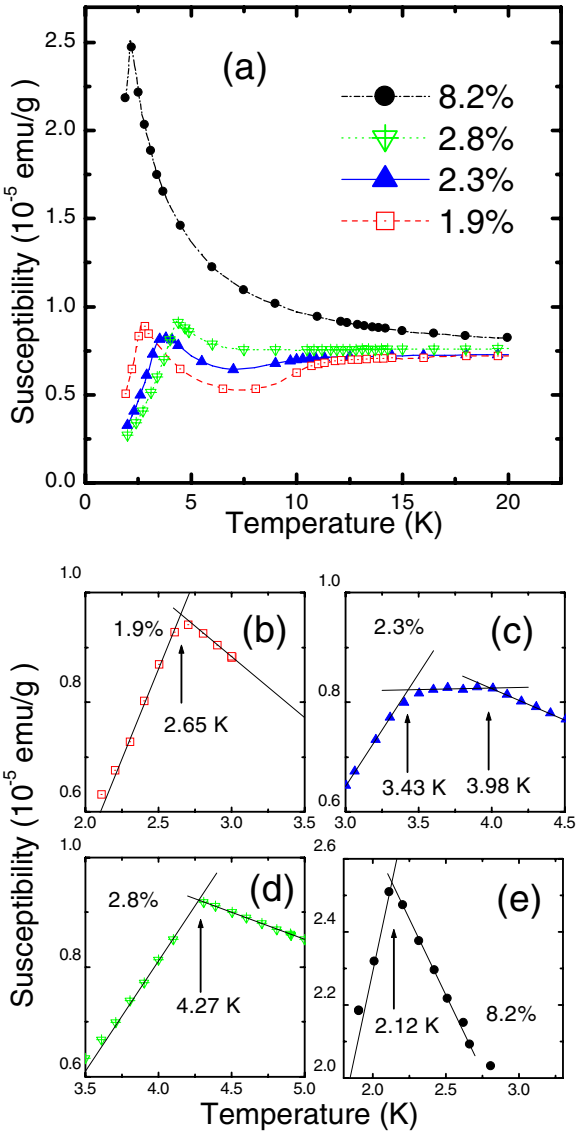

Figure 22. (*a*) $\chi_c(T)$ of $Cu_{1-x}Mg_xGeO_3$ with $x = 0.019$, $0.023(\simeq x_c)$, 0.028 and 0.082. (*b*)–(*e*) $\chi_c(T)$ near T_N. While below and above x_c the cusps are sharp as shown in (*b*), (*d*) and (*e*), at $x \simeq x_c$ the cusp is broad as shown in (*c*). The transition temperatures T_{N1} and T_{N2} were determined at $x = x_c$ as crossing points of three fitted linear functions of T. $T_{N1} = 3.43$ K and $T_{N2} = 3.98$ K in (*c*) (reprinted from [75]).

coexistence of two AF phases. In general the coexistence of phases appears in the case of a first-order phase transition. The data were analysed by fitting three linear functions of T and the crossing points were assigned to the transition temperatures, T_{N1} and T_{N2}. These are T_{N1} = 3.43 K and T_{N2} = 3.98 K at $x = 0.023$ (figure 22(c)). Thus it was concluded that there are two AF phases and that there occurs a first-order phase transition between them [75].

The transition temperatures T_{SP}, T_N (T_{N1} and T_{N2} if there are two transitions) of $Cu_{1-x}Mg_xGeO_3$ are plotted in figure 23 [75]. In the low-concentration region T_N increases

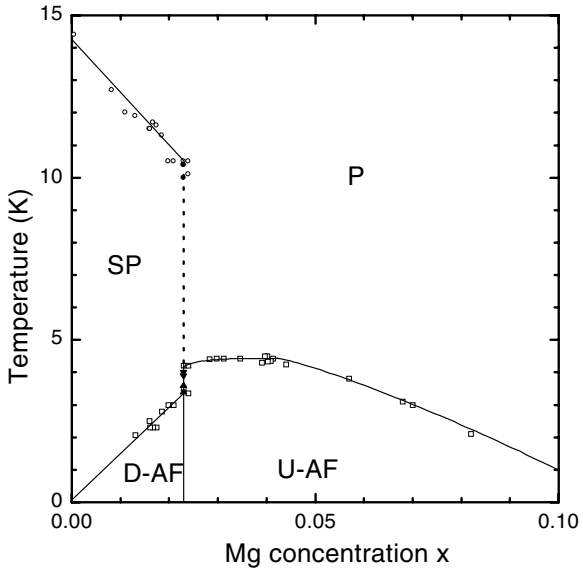

Figure 23. The T–x phase diagram of $Cu_{1-x}Mg_xGeO_3$. Circles and squares indicate T_{SP} and T_N, respectively. At $x = 0.023$ a jump of T_N and sudden disappearance of T_{SP} are observed. Filled triangles represent T_{N1} (upward triangle) and T_{N2} (downward one) at x_c, which are determined as shown in figure 22(c). SP and P indicate spin–Peierls and paramagnetic states. The meanings of DAF and UAF are explained in the text (reprinted from [75]).

smoothly with the concentration of Mg but at $x \simeq 0.023$ it abruptly changes from 3.4 to 4.2 K, corresponding to the existence of a broad peak. Now let us temporarily define this concentration as a critical concentration x_c. A plateau of T_N was observed at $x_c < x \lesssim 0.04$ and a smooth decrease was observed at $0.04 \lesssim x$. T_{SP} reduces linearly from 14.2 K of pure $CuGeO_3$ and disappears near x_c around 10 K.

Figure 23 was explained as follows [75]. The jump of T_N at $x = x_c$ exhibits that AFLROs at $x < x_c$ and $x > x_c$ belong to different phases and there is a first-order phase transition between them. The disappearance of the SP transition at x_c means that in the region of $x > x_c$ the lattice dimerization is absent, i.e. the lattice is uniform. This phase ($x > x_c$ and $T < T_N(x)$) was called the UAF phase in [75]. This phase was supposed to be similar to a conventional AF phase; there is no spatial variation of the staggered moment of spins on Cu^{2+} ions except for the variation directly related to the random distribution of the impurities in contrast to the AF phase in the low-concentration region. At that time in the sample of $x = 0.041$ the absence of dimerization was confirmed by neutron diffraction measurement down to 1.3 K (see [78], also [79] and [80]). On the other hand, as mentioned before, it had been established that in the low-concentration region the AF phase has the dimerization and the AFLRO at the same time [69–71]. Therefore the lattice is dimerized for the $x < x_c$ phase, which was also confirmed by neutron diffraction measurement on the sample of $x = 0.017$ (see [78], also [79] and [80]). There should be spatial variation of the magnitude of spins on Cu^{2+} ions as was claimed in Si-doped $CuGeO_3$ [73]. This phase ($x < x_c$ and $T < T_N$) was called the DAF phase to distinguish it from the UAF phase in [75]. The broad peak of $\chi_c(T)$ in the sample of $x \simeq x_c$ was claimed to indicate that the transition from the DAF phase to the UAF phase is first order as x is varied [75]. The displacement of the Cu^{2+} ion, δ, from a uniform lattice was expected to change abruptly from a finite value to zero at $x = x_c$. The absence of the structural change with x was confirmed by x-ray diffraction at room temperature [75].

The existence of the first-order phase transition between DAF and UAF phases in $Cu_{1-x}Mg_xGeO_3$ has been studied by various experiments, for example neutron diffraction [79–81], synchrotron x-ray diffraction [82–84], a more detailed susceptibility measurement [83] and thermal conductivity measurements [85].

The detailed neutron diffraction experiment of Nakao *et al* revealed the following facts [79, 80]. $T_N(x)$, $\mu^2_{eff}(x)$ and $\delta^2_{eff}(x)/\delta^2_{eff}(0)$ are shown in figure 24 [80]. Here μ_{eff} is the magnetic moment per Cu^{2+} ion and δ_{eff} is the effective atomic displacement. T_N has a discontinuity, $\mu^2_{eff}(x)$ has a large jump and a sharp peak and $\delta^2_{eff}(x)/\delta^2_{eff}(0)$ has a jump at the same concentration, $x_c = 0.027 \pm 0.001$. Thus the first-order phase transition as a function of the concentration was confirmed by the neutron diffraction but the critical concentration was somewhat different from that of [75]. The authors concluded that the actual compositional phase boundary is located higher than $x = 0.023$, namely $x_c = 0.027 \pm 0.001$.

The existence of the AFLRO was also confirmed by their experiments throughout the whole range of concentrations [80]. The superlattice peak (0, 1, 1/2) due to the AFLRO was almost resolution limited in all the samples in spite of the fact that the system contains impurities. The spin–Peierls satellite peak at (3/2, 1, 3/2) was still observed above x_c at $x = 0.028$ and 0.032 but it was not observed at $x = 0.041$. However the peaks of the samples are different between the samples $x > x_c$ and $x < x_c$. One is that the intensity of the (3/2, 1, 3/2) peak of the samples with $x < x_c$ stays at a finite value toward $T = 0$ K, while that of the samples with $x > x_c$ tends to zero toward $T = 0$ K (see figure 25 [80]). The other is that the (3/2, 1, 3/2) peak of the samples with $x > x_c$ has linewidth larger than the instrumental resolution limit (see figure 7 [80]). Therefore in this T–x region the spin–Peierls order is not long range. In a sample in this concentration region the short-range spin–Peierls order develops with decreasing temperature; below T_N it tends to diminish with decreasing temperature and finally vanishes at $T = 0$ K (figure 25 [80]). In this sense the phase transition between DAF and UAF phases is supposed to be a quantum phase transition.

The SP order of $Cu_{1-x}Mg_xGeO_3$ was also studied by means of synchrotron x-ray diffraction by Wang *et al* [82]. They found that the low-temperature SP peak width in the $x = 0.017$ sample is resolution limited, which indicates that the SP state possesses LRO. On the other hand, the SP peaks in the $x = 0.0237$ and 0.026 samples are broadened at all experimentally accessible temperatures, which indicates that only short-range order is present (see figure 26 [82]). The temperature dependences of the peak intensity and the inverse correlation length of the (1.5, 1, 1.5) dimerization peak are plotted in figure 27 [82]. In contrast to pure $CuGeO_3$ the transitions are noticeably rounded for increasing x (figure 27(a) [82]). The peak intensity abruptly decreases around $x \sim 0.025$ (inset of figure 27(a)), which roughly corresponds to x_c of [75]. The low-temperature inverse correlation length as a function of x is shown in the inset of figure 27(b). The system attains LRO only for $x \lesssim 0.021$. Although substantial intensity is observed at the SP peak position for $x > x_c$, the system has only short-range SP order. Therefore they concluded that the phase transition as a function of x reported by Masuda *et al* [75] is characterized by the loss of spin–Peierls long-range order (SP-LRO) at the critical doping x_c. They argued that the structural properties of doped $CuGeO_3$ are determined by impurity-induced competing inter-chain interactions and, possibly, random fields, and therefore are similar to the properties of other systems with competing interactions and/or fields, such as spin-glass and random Ising model compounds [82].

A magnetic susceptibility measurement of $Cu_{1-x}Mg_xGeO_3$ more detailed than the previous one [75] was performed by Masuda *et al* [83]. Clear double cusps were observed (see figure 28 [83]) in the region of $0.0237 \leqslant x \leqslant 0.0271$, which implies the existence of two AF transition temperatures in the samples of this concentration region. The AF

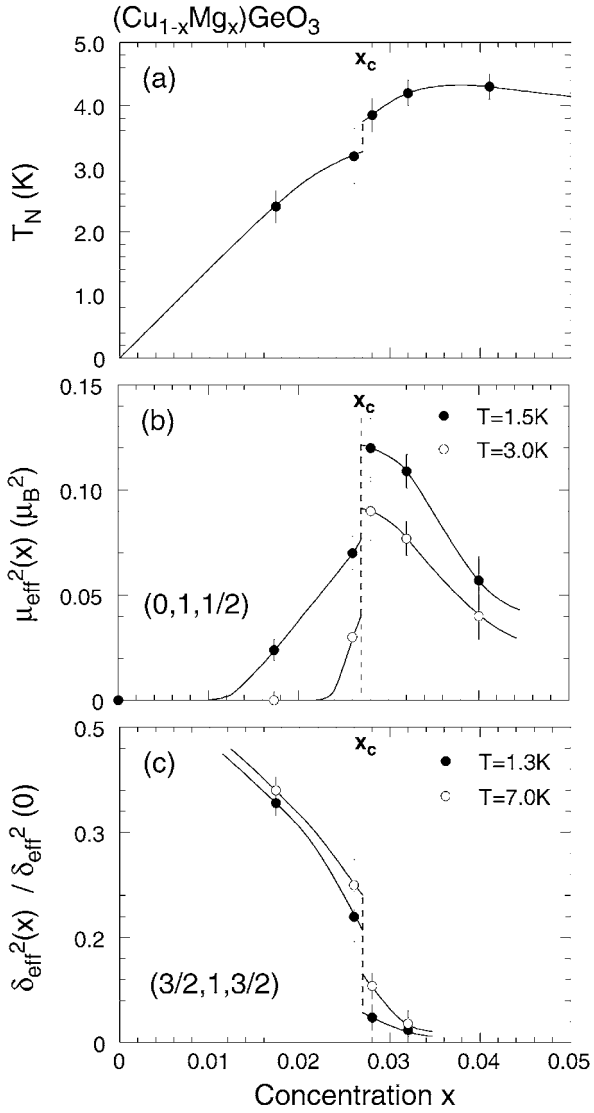

Figure 24. Concentration dependence of (*a*) T_N, (*b*) μ_{eff}^2 at $T = 1.5, 3.0$ K and (*c*) δ_{eff}^2 at $T = 1.3, 7.0$ K. All data clearly show abrupt changes at the critical concentration $x_c = 0.027 \pm 0.001$, evidence for the compositional phase boundary at x_c (reprinted from [80]).

transition temperatures T_{N1}, T_{N2} and T_N are plotted in the vicinity of the critical temperature in figure 29 [83] together with the SP transition temperature T_{SP} observed by the susceptibility measurement. It shows clearly that two AF phases, i.e. DAF and UAF phases, coexist in the region $x_{c1} \leqslant x \leqslant x_{c2}$, where $x_{c1} \sim 0.0237$ and $x_{c2} \sim 0.0271$. The first-order nature of the transition was more clearly exhibited by this observation of the coexistence of the two phases than the jump of T_N reported in [75].

Masuda *et al* [83] summarized the T–x phase diagram of $Cu_{1-x}Mg_xGeO_3$, by considering the results of the susceptibility measurement, synchrotron x-ray diffraction and neutron diffraction. The result is shown in figure 30 [83]. $T_{SP}(\chi_c(T))$ is the SP transition temperature

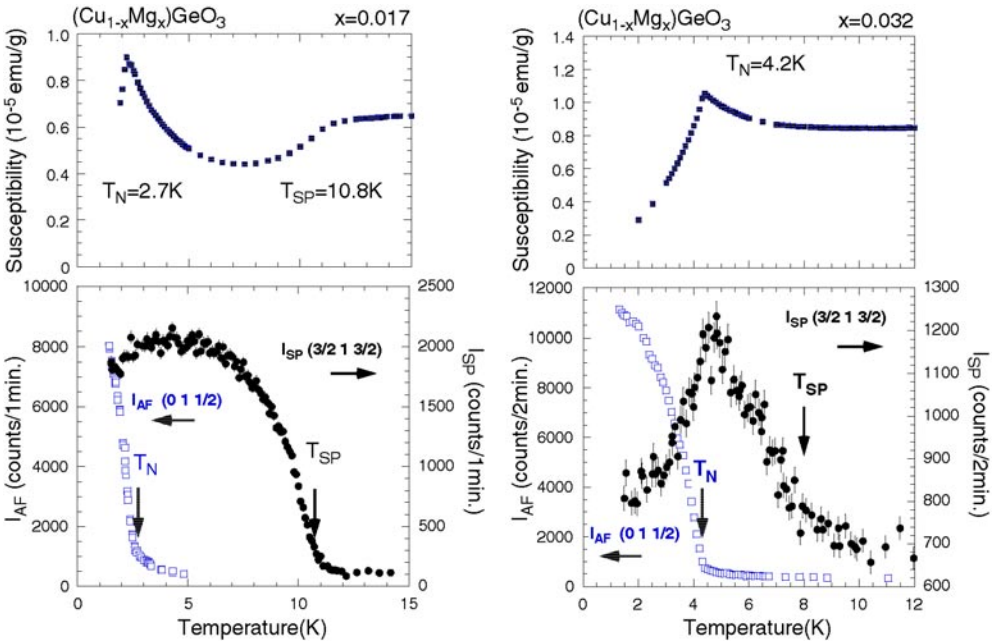

Figure 25. Temperature dependences of the magnetic susceptibilities (top) and the neutron intensities of the superlattice peaks (bottom) of $I_{SP}(3/2\ 1\ 3/2)$ and $I_{AF}(0\ 1\ 1/2)$, respectively, for the samples with $x = 0.017 < x_c$ (left) and $x = 0.032 > x_c$ (right) (reprinted from [80]).

from the susceptibility measurement [83], T_{SP}(neutron) is that from the neutron diffraction experiment of [80] and T'_{SP} (x-ray) is the temperature where the SP correlations become long range [82,83]. Here they have determined T'_{SP} at the temperature where the correlation length of the SP order (dimerization) corresponds to the resolution limit of the synchrotron x-ray measurement, i.e. ∼5000 Å. T'_{SP} decreases with increasing x and vanishes at $x_c \sim 0.024$; i.e., the peak width does not tend to the resolution limit even at the lowest temperature in the $x > x_c$ region [83].

The experimental fact that T'_{SP} is much lower than T_{SP} was explained as follows [83]. The transition temperatures T_{SP} determined from the cusp in $\chi_c(T)$, the anomaly of the heat capacity, and the appearance of the integrated intensity of diffraction at the SP superlattice peak positions coincide with each other. This shows that the correlation length of the dimerization (i.e. phase correlation of the dimerization) of ∼500 Å, which corresponds to the resolution limit of the neutron diffraction, is adequate for the opening of the SP energy gap. On the other hand in pure $CuGeO_3$ T'_{SP} and T_{SP} are the same [87]. The difference is that in the $Cu_{1-x}M_xGeO_3$ system the one-dimensional spin chain is cut at the impurity site. For $T_{SP} > T > T'_{SP}$, the phase of the dimerization is probably pinned at the impurity sites, which is similar to the strong pinning interactions between the impurities and magnetic solitons, which was suggested in the IC phase in $Cu_{1-x}(Zn,Ni)_xGeO_3$ [44]. Only local lattice rearrangements are needed to change the phase at an impurity site. With decreasing temperature the inter-chain interactions and spin–phonon coupling favouring the SP state become relatively more important and the individual finite SP domains begin to correlate with each other over large distances, and at T'_{SP} LRO is finally established.

Kiryukhin *et al* [84] further observed the reentrant nature of the SP transition in the vicinity of x_c by the synchrotron x-ray scattering of Mg-doped $CuGeO_3$. The broadening of the SP

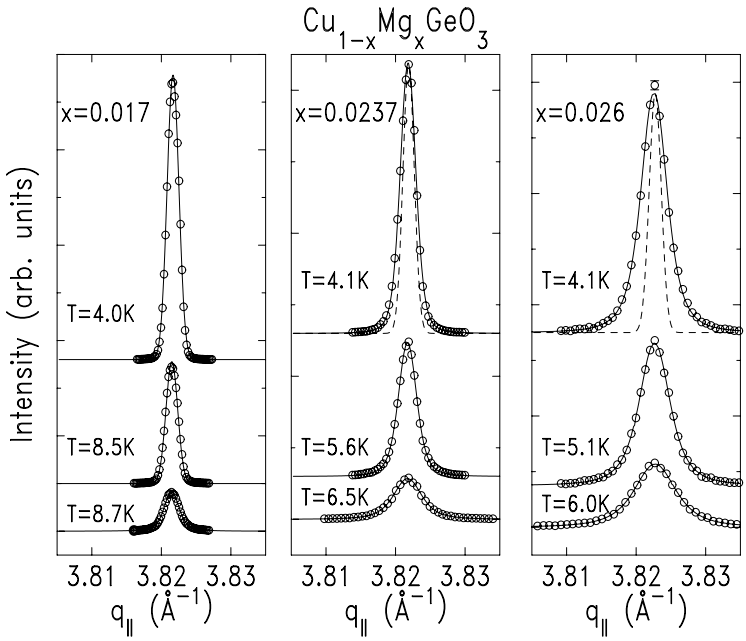

Figure 26. Representative longitudinal scans at the (1.5, 1, 1.5) SP dimerization peak position. The solid curves are the results of fits. The instrumental resolution function is shown as a dashed curve (reprinted from [82]).

dimerization superlattice peaks was observed below the reentrance temperature T_r, which may mean either the complete loss of the long-range SP order or the development of a short-range-ordered component within the long-range-ordered SP state (see figure 31). They also found marked hysteresis and large relaxation times in the samples with $\sim x_c$. The reentrant SP transition was argued to be probably related to the competing Néel transition, which occurs at a temperature where the reentrance occurs. They claimed that the impurity-induced competing interaction discussed in [82] plays an essential role in these phenomena [84].

Recently Nishi *et al* [81] observed the critical scattering due to AF fluctuation near the superlattice reflection (0, 1, 1/2) for samples with $x = 0.024$, 0.026 and 0.029 of $Cu_{1-x}Mg_xGeO_3$, which belong to the same batches as those in [83]. While only the critical scattering due to the T_{N1} transition was observed in $x = 0.024$ and 0.026 samples, a critical scattering due to the T_{N2} transition was strongly observed together with a weak one due to the T_{N1} transition in the sample with $x = 0.029$ (see figure 32 [81]). It was also found that $\mu_{\rm eff}^2$ as a function of x has a large jump (from $\sim$0.08 to $\sim$0.13) at $x \sim 0.028$ and has a maximum for the higher-x side and T_N has a jump near x_c. From these results they concluded that the first-order compositional phase transition between DAF and UAF phases occurs at the critical concentration $x_c = 0.028 \pm 0.001$ [81].

The next problem is whether the first-order compositional phase transition is universal for the impurity-induced AF phase(s) in $CuGeO_3$. The susceptibility measurements of $Cu_{1-x}Ni_xGeO_3$ (Ni^{2+} ion has $S = 1$ spin) by Koide *et al* [64] revealed the disappearance of the SP transition and the abrupt increase of the Néel temperature from 2.5 to 3.4 K at $x \sim 0.020$. This indicates the first-order phase transition between the DAF and the UAF phases [64]. In $Cu_{1-x}Zn_xGeO_3$ (Zn^{2+} ion is nonmagnetic like Mg^{2+} ion) Masuda *et al* [83] observed double cusps in $\chi_c(T)$, although the structure is not so clear as that of $Cu_{1-x}Mg_xGeO_3$

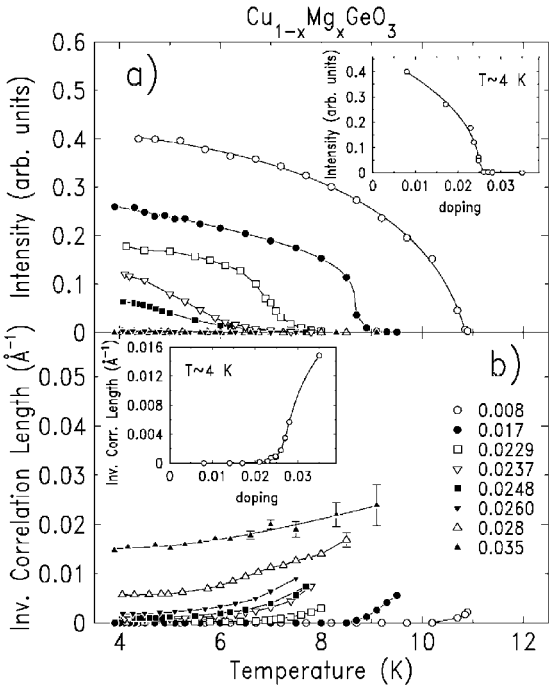

Figure 27. (*a*) The (1.5, 1, 1.5) SP peak intensity and (*b*) the corresponding inverse correlation length as functions of temperature for various Mg-doping concentrations. Insets show (*a*) the impurity-concentration dependence of the low-temperature SP peak intensity and (*b*) the corresponding inverse correlation length. The solid curves are guides to the eye (reprinted from [82]).

(see figure 3 of [83]). This seems to be due to the worse homogeneity of impurity distribution in $Cu_{1-x}Zn_xGeO_3$ compared with that in $Cu_{1-x}Mg_xGeO_3$. In the case of $Cu_{1-x}Zn_xGeO_3$ $x_{c1} \simeq 0.017$ and $x_{c2} \simeq 0.023$ were reported [83]. The first-order phase transition between DAF and UAF phases is probably a universal phenomenon for the substitution for Cu^{2+} ions by either $S = 0$ or $S \neq 0$ impurity ions in $CuGeO_3$.

Another problem is whether this phenomenon appears for the substitution for Ge^{4+} ions by Si^{4+} ions. To study this problem the detailed measurement of the susceptibility of $CuGe_{1-y}Si_yO_3$ was done by Masuda *et al* [88]. It was revealed that double cusps were not observed in $\chi_c(T)$ and that there was no jump of T_N in the T–x phase diagram (see figure 33 [88]). Only a sudden but continuous change in T_N and the disappearance of T_{SP} were confirmed around $x \sim 0.009$, which may imply the existence of a second-order phase transition between DAF and UAF phases. Considering the existence of a first-order phase transition in $Cu_{1-x}Mg_xGeO_3$, $Cu_{1-x}Zn_xGeO_3$ and $Cu_{1-x}Ni_xGeO_3$, this is the first experimental evidence of the qualitative difference of the properties between the substitutions for Cu^{2+} ions and Si^{4+} ions [88]. However there should be other kinds of measurement such as neutron diffraction to reach a firmer conclusion.

Up to now we have explained the phase diagram as a function of impurity concentration. Recent works of Masuda *et al* [89–91] revealed that the magnetic field and pressure can control the phase diagram; i.e., for a sample of fixed impurity concentration we can see the phase transition between the UAF and DAF phases and recovery of the SP transition by applying strong magnetic field [89] or pressure [90, 91].

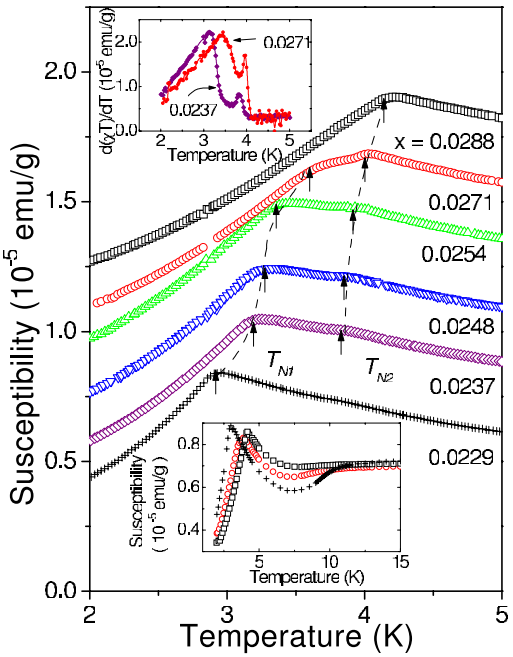

Figure 28. The magnetic susceptibility of $Cu_{1-x}Mg_xGeO_3$ near the AF transition temperature(s). The applied field was 1000 Oe. The data of different x are shifted vertically. Double cusps are observed in the region of $0.0237 \lesssim x \lesssim 0.0271$, while a single cusp is observed in the regions of $x < 0.023$ and $0.028 < x$. The arrows indicate the anomaly due to the AF transition. The inset in the upper left is $\partial(\chi_c T)/\partial T$ for determining T_{N1} and T_{N2} according to Fisher's theory [86]. The inset at the bottom shows the magnetic susceptibility in the same samples of $x = 0.0271$, 0.0288 and 0.0299 for 2 K $< x <$ 20 K (reprinted from [83]).

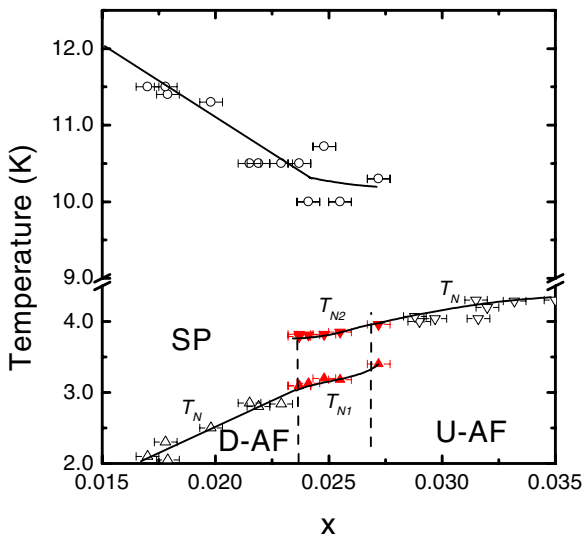

Figure 29. The temperature versus concentration phase diagram determined by the magnetic susceptibility measurement. Open circles and triangles and closed upward and downward triangles are T_{SP}, T_N, $T_{N1}$and T_{N2}, respectively (reprinted from [83]).

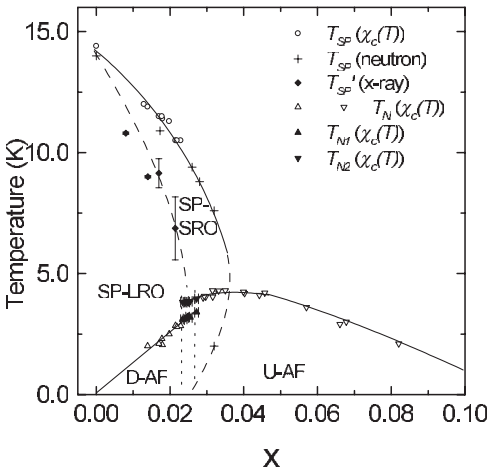

Figure 30. T–x phase diagram of $Cu_{1-x}Mg_xGeO_3$ produced by susceptibility measurements, x-ray diffraction and neutron diffraction. DAF, UAF, SP-LRO and SP-SRO denote the DAF phase, UAF phase, SP long-range order and SP short-range order, respectively. Neutron diffraction data are from figure 6 of [80] (reprinted from [83]).

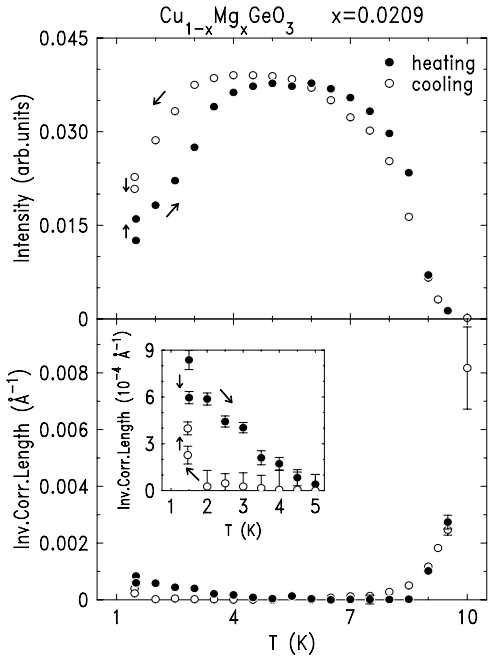

Figure 31. Temperature dependence of the (1.5, 1, 1.5) SP peak intensity (top panel) and the corresponding longitudinal inverse correlation length (bottom panel) taken on heating and on cooling in the $x = 0.0209$ sample. The inset shows the low-temperature inverse correlation length (reprinted from [84]).

4.3. Antiferromagnetic phase in the extremely-low-concentration region

In this subsection I shall discuss to how low concentration the AF phase continues to exist.

The experiment was performed by Manabe *et al* [76] using $Cu_{1-x}Zn_xGeO_3$ single-crystal samples with the concentration down to $x = 1.12 \times 10^{-3}$. Since T_N decreases with decreasing

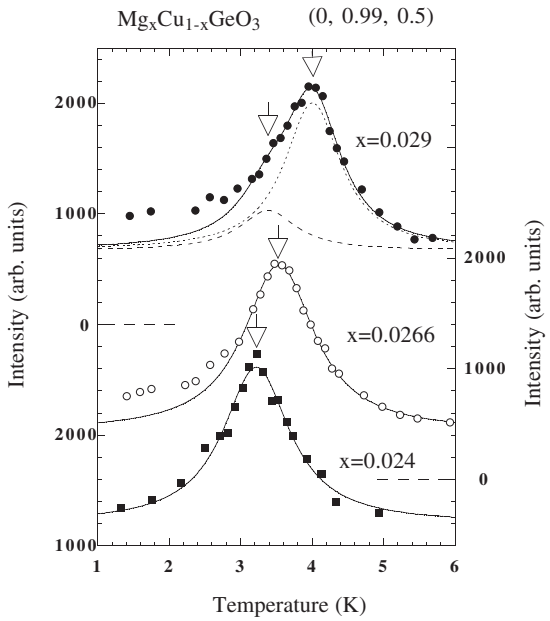

Figure 32. Critical neutron scattering observed at (0, 0.99, 0.5) near the AF Néel points. Intensity differences from the solid curve on the low-temperature side of $x = 0.0266$ and 0.029 are contributed by the foot of the (0, 1, 0.5) Bragg peak. Empty arrows indicate the divergent positions of the critical scattering intensity (reprinted from [81]).

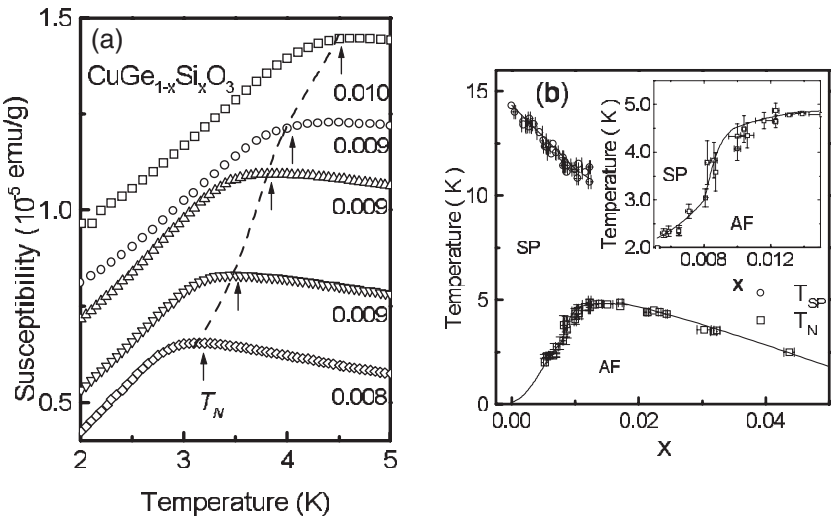

Figure 33. (*a*) The magnetic susceptibility and (*b*) the temperature–concentration (T–x) phase diagram of $CuGe_{1-y}Si_yO_3$ (reprinted from [88]).

concentration, the magnetic susceptibilities were measured down to 5 mK using a combination of a ^{3}He–^{4}He dilution refrigerator and a $PrNi_5$ adiabatic demagnetization refrigerator.

In figure 34 $\chi_c(T)$ for various x samples (including undoped $CuGeO_3$) are shown [76]. The direction of the easy axis (parallel to the c axis) of the AF phase was confirmed not to

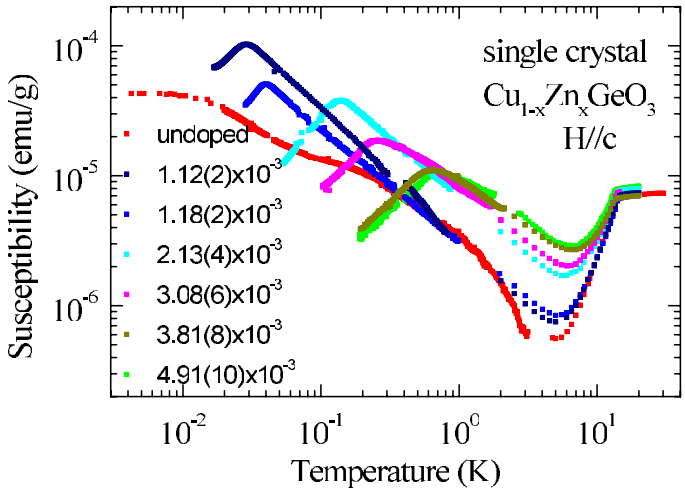

Figure 34. The temperature dependence of $\chi_c(T)$ of the single-crystal $Cu_{1-x}Zn_xGeO_3$ with $x < 5 \times 10^{-3}$ in AC magnetic field. Numerals denote the Zn concentrations x (reprinted from [76]).

change in the $x = 1.18(2) \times 10^{-3}$ sample (see figure 1 of [76]) and therefore the measurements were made only for $\boldsymbol{H} \parallel c$-axis for other samples. As for the undoped sample it was expected that the concentration of impurities or defects was extremely low but even this may contain defects which play a similar role as Zn^{2+} ions. Both the defects cut the dimerized chains of Cu^{2+} and can produce nearly isolated $S = 1/2$ states on the edges of the segments as nonmagnetic impurities. The concentration of defects or impurities was estimated by the Curie–Weiss fitting. The difference of the concentration estimated by the inductively coupled plasma atomic emission spectroscopy (ICPAES) and that estimated by the Curie–Weiss fitting was less than 20% in the low-Zn-concentration region ($x < 5 \times 10^{-3}$) (see figure 3 of [76]). Thus the validity of the determination of Zn concentration was confirmed. The fitting gives an effective value of the concentration as $x = 2.3(2) \times 10^{-4}$ for the undoped sample. Its susceptibility seems to saturate below 12 mK (figure 34). There are two possible reasons for the occurrence of this saturation. One is that the undoped sample was not cooled below 0.012 K. The other is that the susceptibility is indeed constant below 12 mK, which implies that the AF transition occurs below 12 mK. Which is the real case was not determined. In any case the AF transition does not occur above 12 mK in the undoped sample.

The spin–Peierls transition temperature, T_{SP}, and the Néel temperature, T_N, as functions of Zn concentration are shown in figure 35 [76]. The behaviour of T_N in the very-low-concentration region and the appearance of the AF transition at 28.5 mK for such a low Zn concentration as $x = 1.12(2) \times 10^{-3}$ imply that there is no critical concentration for the occurrence of the AFLRO. In fact T_N can be fitted to a formula

$$T_N = A \exp(-B/x), \tag{4.1}$$

for low Zn concentration ($1.12(2) \times 10^{-3} \leqslant x \leqslant 4.91(10) \times 10^{-3}$). The parameters were obtained as $A = 2.3$ K and $B = 5.7 \times 10^{-3}$. According to equation (4.1) T_N is estimated to be 1 mK or lower for the undoped sample (effectively $x = 2.3(2) \times 10^{-4}$). This is consistent with our failure to observe an AF transition for the undoped sample.

This may arise from the fact that the dimerization sustains the phase coherence of the spin polarization, although it suppresses the magnitude of the spin polarization. The absence of critical concentration is also consistent with the theory of the impurity-doped SP system [73].

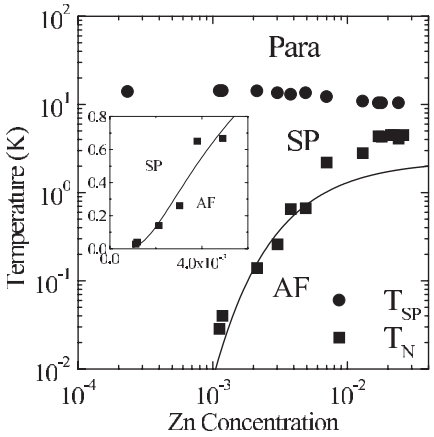

Figure 35. T_N and T_{SP} as functions of Zn concentration x. Para, SP and AF represent paramagnetic, spin–Peierls and antiferromagnetic states, respectively. The solid curve is that best fitted by equation (4.1). The inset shows the same relation in the low-concentration region in linear scales (reprinted from [76]).

5. Spin gap and the impurity-induced ordered phase in other low-dimensional spin systems

On $CuGeO_3$ there have been many studies related to the impurity-induced AF states as we have seen in the previous sections. Here there occurs a problem: whether the impurity-induced AF phase is unique to the $S = 1/2$ spin-gap systems such as spin–Peierls $CuGeO_3$ or two-leg spin ladder $SrCu_2O_3$ [92] or not. As to $SrCu_2O_3$ see the later sections. Another typical spin-gap system is the Haldane-gap system with $S = 1$ spins [3]. So we have tried to reveal whether the Haldane-gap system can have an impurity-induced AF phase or not.

5.1. A new Haldane compound $PbNi_2V_2O_8$

When we began to study this problem, there had been no papers which reported the impurity-induced AF phase in a Haldane-gap system. Therefore it was necessary to search for new $S = 1$ spin materials. The first candidate was $SrNi_2V_2O_8$, whose crystal structure was reported by Wickmann and Müller-Buschbaum in 1986 [93]. The susceptibility versus temperature measured by Uchiyama [94] showed that it has the characteristic of a Haldane system above 6.5 K but has an ordered state below this [94, 95].

Then $PbNi_2V_2O_8$ was studied. This was a new material, whose crystal structure had not been reported. Uchiyama *et al* [77] found out that the structure of $PbNi_2V_2O_8$ is isomorphic to that of $SrNi_2V_2O_8$ (see the inset of figure 36). The structure of $PbNi_2V_2O_8$ is tetragonal, the space group is $I4_1cd$ and the lattice parameters are $a = 12.249(3)$ Å and $c = 8.354(2)$ Å. The slightly distorted NiO_6 octahedra are edge shared around the fourfold screw axis along the c axis. All the $S = 1$ Ni^{2+} ions, as well as all the nn Ni^{2+}–Ni^{2+} bonds, are equivalent. The screw chains are separated by VO_4 tetrahedra and Pb^{2+} ions. Intra-chain nn Ni–Ni AF interactions are expected to dominate. The V^{5+} sites are presumed to be nonmagnetic. The experiments were performed on powder samples. The anisotropic properties were measured on the samples, which were aligned in magnetic fields of 9–13.2 T.

The temperature dependences of the susceptibilities $\chi(T)$ of highly aligned (at 9 T) samples are shown in figure 36 [77]. The susceptibilities in the magnetic field parallel and

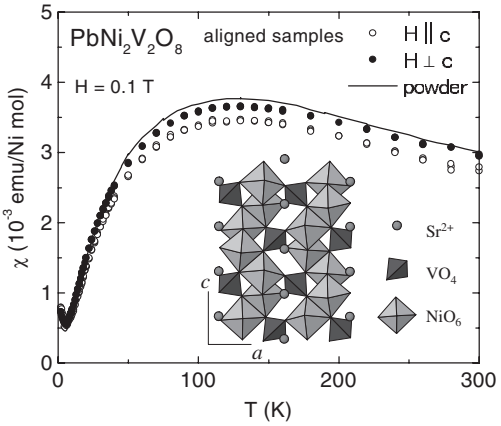

Figure 36. Temperature dependence of magnetic susceptibility measured in $PbNi_2V_2O_8$. The solid curve shows data for a nonaligned powder sample. The symbols are for highly aligned polycrystalline samples. The magnitudes of data for aligned samples are not exact because we cannot exactly estimate the quantity of powder contained in the resin. The true magnitude for $\boldsymbol{H} \parallel c$-axis should be larger than that for $\boldsymbol{H} \perp c$-axis because of the c-axis alignment. Inset: a schematic view of the crystal structure of $(Sr/Pb)Ni_2V_2O_8$ according to [93] (reprinted from [77]).

perpendicular to the magnetic field are almost the same: the anisotropy of the susceptibility is very small. $\chi(T)$ has a broad maximum around 120 K. Below this temperature $\chi(T)$ decreases exponentially to almost zero. This indicates that the ground state is a spin-singlet state and the energy gap exists between the ground state and the excited states. A small upturn of the susceptibility near the lowest temperature can be attributed to the presence of paramagnetic impurities. A straightforward analysis of the data collected in the range $0 < T < 40$ K yielded the thermal activation energies: $\Delta = 29.4$ K $= 2.53$ meV for $\boldsymbol{H} \parallel \boldsymbol{c}$ and $\Delta = 27.8$ K $= 2.39$ meV for $\boldsymbol{H} \perp \boldsymbol{c}$. High-field magnetization data were also taken on aligned polycrystalline samples in magnetic fields of up to 40 T. Figure 37 [77] shows magnetization curves measured at $T = 4.2$ K. At high fields an abrupt change of slope in $M(H)$ is observed for both $\boldsymbol{H} \parallel \boldsymbol{c}$ and $\boldsymbol{H} \perp \boldsymbol{c}$. The corresponding critical fields were $H_c^{\perp} = 14$ T and $H_c^{\parallel} = 19$ T.

The activation-type temperature dependence of the susceptibility and the anomalous behaviour of the magnetization versus magnetic field are clear evidence of a nonmagnetic ground state and the spin-gap excitation. Although the arrangement of $S = 1$ Ni^{2+} ions is not straight but is a fourfold screw chain, their one-dimensional arrangement strongly suggests that $PbNi_2V_2O_8$ is a Haldane antiferromagnet. Then the starting point to describe this system is as follows: under the assumption of a purely one-dimensional $S = 1$ spin system the intra-chain interaction is assumed to be isotropic and is expressed as

$$\hat{H}_{\text{in-chain}} = J \sum_{i,k} \boldsymbol{S}_{i,k} \cdot \boldsymbol{S}_{i+1,k}, \tag{5.1}$$

and in addition an effective single-ion term

$$\hat{H}_{\text{single-ion}} = D \sum_{i,k} (S_{i,k}^z)^2, \tag{5.2}$$

is considered. Here i describes the ith spin in the kth screw chain. For a small D the ground state is a Haldane singlet and the lowest excitations are a singlet of a longitudinal mode and a doublet of transverse-polarized Haldane excitations. A simple application of equation (2.14) in [96] to $PbNi_2V_2O_8$, which relates the critical fields $H_c^{\perp}$ and $H_c^{\parallel}$ to the

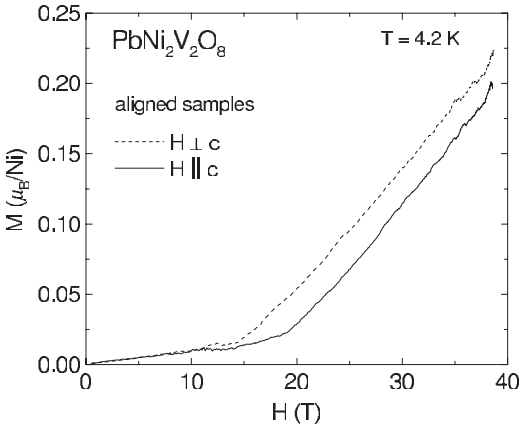

Figure 37. Magnetization curves measured in $PbNi_2V_2O_8$ at $T = 4.2$ K for magnetic fields parallel and perpendicular to the chain axis (reprinted from [77]).

doublet and singlet gap energies $\Delta_\perp$ and $\Delta_\parallel$ in a purely one-dimensional $S = 1$ system, produces the following results: $\Delta_\perp = 2.2$ meV and $\Delta_\parallel = 1.2$ meV. The intra-chain exchange constant J was also deduced from the high-temperature part of the measured $\chi(T)$ curves according to [97] and this analysis yields $J = 95$ K $= 8.2$ meV. The obtained mean gap energy $(2\Delta_\perp + \Delta_\parallel)/3 = 1.87$ meV is substantially smaller than the value $0.41J \approx 3.36$ meV expected for noninteracting chains [96, 100]. The large difference between the experimental and theoretical gap energies was attributed to the inter-chain exchange interactions. In their presence the excitation energies depend on the dispersion in the reciprocal space perpendicular to the chain axis. In this case $\Delta_\perp$ and $\Delta_\parallel$ represent the global minima in the three-dimensional dispersion, and cannot be uniquely related to J [77].

Dynamic spin correlations in $PbNi_2V_2O_8$ and $SrNi_2V_2O_8$ were studied in a series of inelastic neutron scattering experiments on powder samples [77, 95, 98]. Examples of the neutron scattering experiments are shown in figure 38 [95].

Because of the powder sample the dispersion relation of spin excitations was not derived directly from these experiments. Therefore the data were fitted with the model cross section calculated by the Monte Carlo algorithm and the best fitted parameters were obtained. The model Hamiltonian expressing the spin state was taken as the intra-chain interaction equation (5.1) plus the single-ion term equation (5.2) and the inter-chain interaction

$$\hat{H}_{\text{inter-chain}} = \sum_{i,i',k,k'} [J_{1,\parallel} S^z_{i,k} S^z_{i',k'} + J_{1,\perp}\{S^x_{i,k} S^x_{i',k'} + S^y_{i,k} S^y_{i',k'}\}]. \tag{5.3}$$

Here the sum is taken over pairs of nn spins between the adjacent chains [95].

Noninteracting susceptibility for an isolated chain was treated by the single-mode approximation (SMA). The effect of the inter-chain interaction was treated by the chain mean-field random phase approximation (RPA). Because of the complex chain structure (screw chain) the method is very complicated and the details are left to [95]. Comparing the calculation and the experimental data the adjustable parameters were determined. For $PbNi_2V_2O_8$ the parameters are two intrinsic gap energies $\Delta_\parallel$ and $\Delta_\perp$, and the doublet three-dimensional gap $E_{\min,\perp}$. The singlet three-dimensional gap was fixed to $E_{\min,\parallel} = 1.2$ meV, as determined in high-field bulk measurements as mentioned above [77]. The least-squares refinement yielded: $\Delta_\perp = 4.0 \pm 0.25$ meV, $\Delta_\parallel = 3.1 \pm 0.3$ meV and $E_{\min,\perp} = 2.4 \pm 0.2$ meV ($J_1 < 0$), with $\chi^2 = 2.3$ [95].

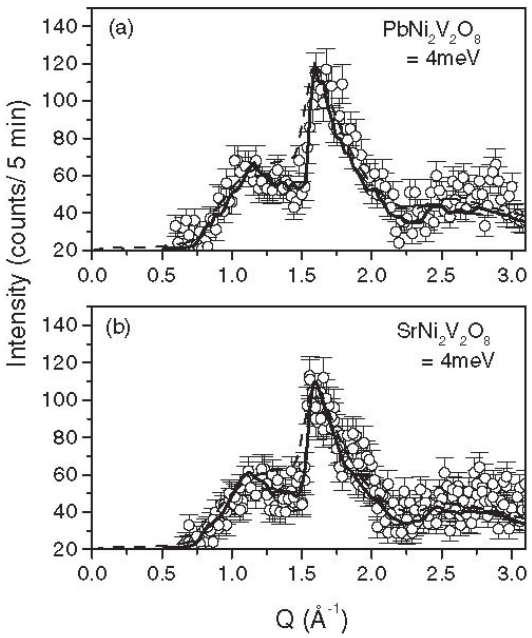

Figure 38. Constant-energy scans measured in (*a*) $PbNi_2V_2O_8$ and (*b*) $SrNi_2V_2O_8$ powder samples at $T = 2$ K in the standard three-axis mode. The solid curves are simulations based on parameters obtained in a global fit to the data. Dashed lines are similar simulations for non-interacting spiral-shaped spin chains (reprinted from [95]).

In this approximation the relations between the actual gaps (excitation energies at the three-dimensional AF zone centre) and the intrinsic gaps are expressed as follows:

$$E^2_{\min,\perp} = \Delta^2_\perp - 2Zv|J_{1,\perp}|, \tag{5.4}$$

$$E^2_{\min,\parallel} = \Delta^2_\parallel - 2Zv|J_{1,\parallel}|. \tag{5.5}$$

Here $v = 2.49J$ is the spin-wave velocity and $Z = 1.26$ [99]. The parameters $E_{\min,\perp}$ and $E_{\min,\parallel}$ depend only on the absolute values of $J_{1,\perp}$ and $J_{1,\parallel}$. However, the sign of these parameters explicitly enters the dispersion relation and thus directly affects neutron scattering intensity versus k and can be determined. The obtained values are $J_{1,\perp} = -0.18$ meV and $J_{1,\parallel} = -0.14$ meV [95]. $|J_1|$ is larger by a factor of 1.5–2 compared with the previous estimate ($|J_\perp| = 0.096 \pm 0.003$ meV) in [77]. This discrepancy should be partly attributed to a difference in the definition of J_1. In the previous model each spin was postulated to be coupled to four spins in adjacent chains (coordination number 4). In the more realistic model in [95] the inter-chain coordination number is 2. This automatically translates into a factor of two for $|J_1|$ within the random phase approximation. The sign is reversed compared with the previous one [77], because the inter-chain interaction exists between the Ni^{2+} ions with different heights along the c direction (by $c/4$, i.e. one step in a fourfold screw). The minus sign of $J_{1,\parallel}$ and $J_{1,\perp}$ means that the inter-chain interaction is effectively AF in the same c plane.

From the refined $\Delta_\perp$ and $\Delta_\parallel$ the intra-chain coupling constant $J \approx 9.0$ meV was obtained. This value is in better agreement with the high-temperature susceptibility estimate $J \approx 8.2$ meV in [77] than the preliminary neutron result $J = 9.5$ meV, from the same reference. The single-ion anisotropy D can be estimated from $\Delta_\perp$ and $\Delta_\parallel$ using

$$\Delta_\perp = \langle\Delta\rangle - 0.57D, \tag{5.6}$$

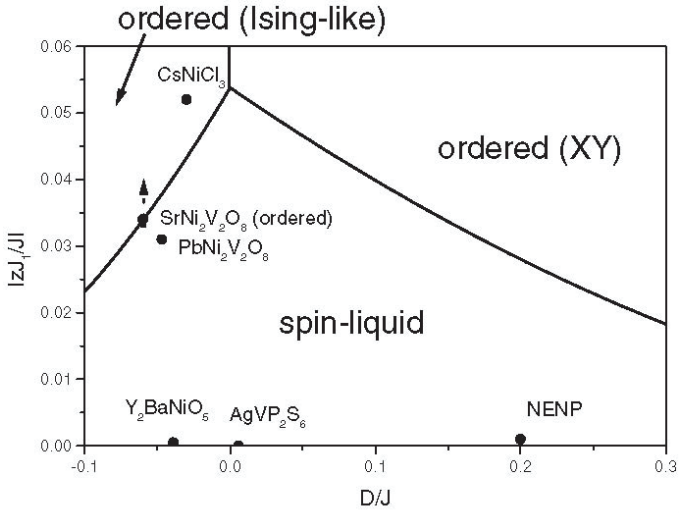

Figure 39. D–J_1 phase diagram for weakly coupled Haldane spin chains [100], showing the location of some well characterized quasi-one-dimensional $S = 1$ systems. $CsNiCl_3$ data from [101]; Y_2BaNiO_5 data from [102]; NENP data from [103]; $AgVP_2S_6$ data from [104]; $PbNi_2V_2O_8$ and $SrNi_2V_2O_8$ are placed based on the results of [95]. The vertical arrow indicates that the $SrNi_2V_2O_8$ compound must be actually deeper in the ordered phase than suggested by the analysis (reprinted from [95]).

$$\Delta_{\parallel} = \langle\Delta\rangle + 1.41D. \tag{5.7}$$

An additional relation is the mean intrinsic Haldane gap $\langle\Delta\rangle \approx (\Delta_{\parallel} + 2\Delta_{\perp})/3$. This parameter is, to a good approximation, defined by J alone: $\langle\Delta\rangle \approx 0.41J$. Using these relations $D = -0.45$ meV was obtained for $PbNi_2V_2O_8$ [95].

The results for $PbNi_2V_2O_8$ and $SrNi_2V_2O_8$ are summarized in the phase diagram of inter-chain interaction $|zJ_1/J|$ versus single-ion interaction D/J (figure 39). Here z is the number of nn chains (see the above explanation, in this case $z = 2$) and the absolute value of zJ_1/J is plotted, because $J_1 < 0$ is effectively AF interaction as explained before. In this figure solid curves are the theoretical calculation of Sakai and Takahashi [100]. Their theory treated the inter-chain interaction by the chain mean-field theory, which roughly corresponds to the analysis of the experiment in [95]. The ground state of $SrNi_2V_2O_8$ is located in the Ising-like ordered state but it may be very close to the boundary between the Haldane (spin-liquid) phase and the Ising-like AF phase. On the other hand the ground state of $PbNi_2V_2O_8$ turned out to be very close to the boundary but in the Haldane phase. $CeNiCl_3$ [101] is located definitely in the Ising-like AF phase but not far from the boundary. On the other hand the well known Haldane materials Y_2BaNiO_5 [102], NENP [103] and $AgVP_2S_6$ [104] are situated deep in the Haldane phase.

The magnetic excitations in $PbNi_2V_2O_8$ and $SrNi_2V_2O_8$ were measured up to the zone boundary energy using inelastic neutron scattering from powder samples [98]. In this paper an estimate of the next-nn intra-chain interaction was obtained.

It was revealed that the characteristic properties of $PbNi_2V_2O_8$ are that it is a Haldane-gap material and, on the other hand, it has a strong inter-chain interaction barely sustaining the spin gap. This reminds us that $CuGeO_3$ also has strong inter-chain interaction. Then the next problem is the impurity effect. Is there any similarity between the impurity effects of $CuGeO_3$ ($S = 1/2$ spin system) and $PbNi_2V_2O_8$ ($S = 1$ spin system)?

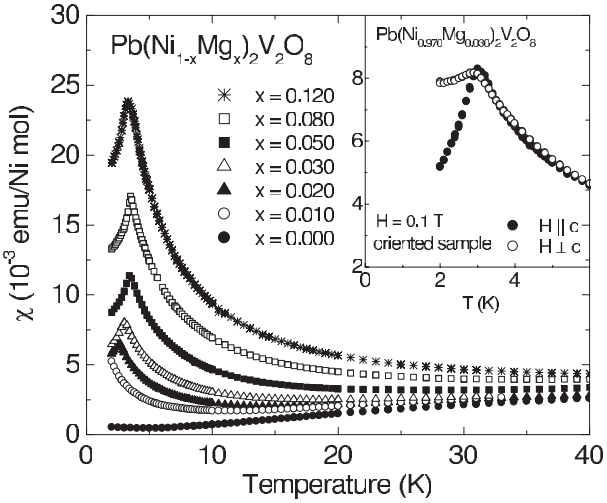

Figure 40. Temperature dependences of magnetic susceptibility measured in $Pb(Ni_{1-x}Mg_x)_2V_2O_8$ ($0 \leqslant x \leqslant 0.120$) powder samples. The inset shows the data for highly aligned $Pb(Ni_{0.970}Mg_{0.030})_2V_2O_8$ (reprinted from [77]).

5.2. Impurity-induced ordered phase in $PbNi_2V_2O_8$

The main subject of this subsection is to find whether impurities induce the AF phase or more generally an ordered phase in a Haldane system, particularly, in $PbNi_2V_2O_8$. First the substitution of nonmagnetic Mg^{2+} ions for $S = 1$ Ni^{2+} ions was tried. This will introduce a spin vacancy in the $S = 1$ screw spin chain. The temperature dependences of magnetic susceptibility for a series of $Pb(Ni_{1-x}Mg_x)_2V_2O_8$ powder samples with $x = 0$–0.120 are shown in figure 40 [77]. In the $x = 0$ compound gap behaviour is observed as discussed before. In contrast an increase of susceptibility is observed at low temperatures in all doped samples. The enhancement scales with Mg concentration, and can be attributed to the presence of free $S = 1/2$ spins at the ends of the Ni chains cut by the spin vacancies [99]. The occurrence of the $S = 1/2$ 'edge spins' around both sides of the spin vacancies can be well explained by the valence bond solid (VBS) model [105] and also established by numerical calculation [106]. Experimentally Hagiwara *et al* [107] confirmed this phenomenon by measuring the ESR of the $S = 1$ linear-chain Heisenberg antiferromagnet $Ni(C_2H_8N_2)_2NO_2(ClO_4)$, i.e. NENP, whose Ni^{2+} ions are partially replaced by $S = 1/2$ Cu^{2+} ions. In this model the number of liberated spins is twice the number of spin vacancies. In the experiment of $PbNi_2V_2O_8$ [77] the temperature dependence of magnetic susceptibility in $Mg^{2+}(S = 0)$- and $Cu^{2+}(S = 1/2)$-substituted samples was measured. The substitution of a Cu^{2+} ion for a Ni^{2+} ion also produces two edge spins. However, if these two spins couple antiferromagnetically to the Cu spin, the three coupled spins produce a ground-state configuration of total spin $S = 1/2$. Then the total number of added $S = 1/2$ free spins is equal to the total number of added $S = 1/2$ ions. Experimentally, the measured $\chi(T)$ curve for a 2.0% Cu-doped $PbNi_2V_2O_8$ sample (above the kink) (not shown in figure 40) was found to be equal to that for a 1.0% Mg-doped sample in figure 40. This shows that the edge spin model due to the VBS model can be applied to doped $PbNi_2V_2O_8$, which has a strong inter-chain interaction, even up to several per cent substitution.

The most important finding of Uchiyama *et al* in [77] is the observation of an anomaly in the magnetic susceptibility of $Pb(Ni_{1-x}Mg_x)_2V_2O_8$ below $T_c \approx 3.5$ K for $x \geqslant 0.020$. The

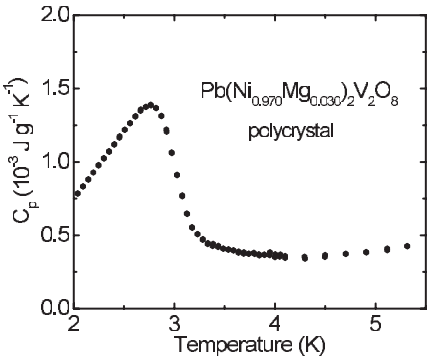

Figure 41. An example of the heat-capacity measurements. The sample is $Pb(Ni_{0.970}Mg_{0.030})_2V_2O_8$ (reprinted from [108]).

slope of $\chi(T)$ changes abruptly with reversal of sign. This behaviour indicates clearly the existence of a magnetic phase transition.

The next problem was to what kind of phase transition this anomaly corresponds. The anisotropic behaviour of the susceptibility was studied using aligned samples of $x = 0.030$ with the transition temperature of about $T_N = 3.0$ K (see the inset of figure 40). Below T_N a large anisotropy of susceptibility is observed. For $\boldsymbol{H} \parallel c$, $\chi(T)$ decreases abruptly below T_N. In contrast, for $\boldsymbol{H} \perp c$ it remains practically constant. This behaviour is typical of a Néel antiferromagnet with easy axis along the c direction. These facts clearly show that the new phase is the AF phase. The existence of the phase transition was also confirmed by the measurement of the heat capacity. Figure 41 [108] shows the measurement of the heat capacity $C_p(T)$ on $Pb(Ni_{0.970}Mg_{0.030})_2V_2O_8$. $C_p(T)$ has an anomaly apparently due to a phase transition. This experiment undoubtedly shows the existence of the spin-vacancy-induced AF phase in this system.

The effect of substitution has been studied experimentally (see, for example, [107]) and theoretically [105] for a number of Haldane-gap systems as mentioned already. Apart from the appearance of edge spins and the resulting paramagnetic contribution to the low-T susceptibility, the finite length of the chains leads to a reduction of the dynamic spin correlation length. $PbNi_2V_2O_8$ is the first example of a Haldane antiferromagnet that orders magnetically by doping. Here the role of the inter-chain interactions is important. To order magnetically the spins must be coupled in three-dimensional space. As we have demonstrated, inter-chain coupling is quite substantial in $PbNi_2V_2O_8$. The possibility of vacancy-induced LRO in a Haldane-gap system was first qualitatively discussed by Shender and Kivelson [109]. In particular, the authors suggested that there is a critical impurity concentration below which LRO does not occur. As to this point more detailed low-T studies are required.

We should not confuse the magnetic transition observed in $Pb(Ni_{1-x}Mg_x)_2V_2O_8$ with that in the extensively studied Haldane-like system $CsNiCl_3$ [110–112]. As shown in figure 39, the direct inter-chain interactions in $CsNiCl_3$ are stronger than the critical value, unlike the case in $PbNi_2V_2O_8$ and even pure $CsNiCl_3$ has a magnetically ordered ground state. The substitution of Mg^{2+} ions for Ni^{2+} ions leads to a decrease of the ordering temperature [113], which is in striking contrast with the behaviour of $PbNi_2V_2O_8$.

The T–x phase diagram was obtained by measurements of the susceptibility and heat capacity of the samples with various concentrations. Figure 42 [108] shows that the transition

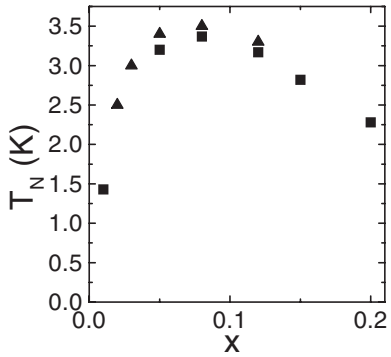

Figure 42. T_N–x relation in $Pb(Ni_{1-x}Mg_x)_2V_2O_8$. Triangles and squares are from the maxima of $\chi(T)$ and $C_p(T)$, respectively (reprinted from [108]).

temperature T_N has a tendency to rise steeply, has a maximum value of about 3.5 K near $x = 0.08$ and slowly decreases above it. This behaviour is very similar to that of SP $CuGeO_3$ doped with Zn, Mg or Ni for Cu or Si for Ge as was discussed in the previous section and the two-leg ladder system $SrCu_2O_3$ [92]. The behaviour shown in this figure suggests that there may be no critical concentration for the occurrence of the AF phase in this system as in the case of $CuGeO_3$, but before we reach a firm conclusion it is necessary to perform the measurements on the more lightly doped samples, which needs the measurements at much lower temperature as was done for $CuGeO_3$ [76].

In $CuGeO_3$ the in-chain substitutions of nonmagnetic ($S = 0$ Mg^{2+} ion, Zn^{2+} ion) or magnetic ($S = 1$ Ni^{2+} ion, $S = 5/2$ Mn^{2+} ion) ions for $S = 1/2$ Cu^{2+} ions in the chain as well as the off-chain nonmagnetic ($S = 0$) Si^{4+} ion substitution for nonmagnetic ($S = 0$) Ge^{4+} ion causes essentially the same AF phase at least in the low-concentration region as was discussed in the previous section. Therefore it is very interesting to know how the phase transition varies with impurity species in $PbNi_2V_2O_8$.

First it was proved that the spin vacancy induces the AF phase irrespective of the impurity species. The susceptibilities of $Mg^{2+}(S = 0)$- and $Zn^{2+}(S = 0)$-doped $PbNi_2V_2O_8$ samples were measured and it was found that T_N and the magnitude of the Curie terms induced by the doping are almost the same for the same concentrations [114]. This confirms that spin vacancies really induce the AF phase.

Previously it was written that the measured $\chi(T)$ curve for a 2% Cu-doped $PbNi_2V_2O_8$ sample (above the kink) ($S = 1/2$ Cu^{2+} ion) was found to be equal to that for a 1.0% Mg-doped sample and this shows that the edge spin model due to the VBS model can be applied to $PbNi_2V_2O_8$ [77]. It was naturally expected that the $Pb(Ni_{1-x}Cu_x)_2V_2O_8$ sample with the Cu concentration of twice the Mg concentration of $Pb(Ni_{1-x}Mg_x)_2V_2O_8$ might have the same transition temperature as the latter sample. However as shown in figure 43 [114] $Pb(Ni_{1-x}Cu_x)_2V_2O_8$ with $x = 0.040$ does not show a transition in the temperature region where the $Pb(Ni_{1-x}Mg_x)_2V_2O_8$ sample with $x = 0.020$ does ($T_N \sim 2.5$ K) nor down to 0.4 K (not shown in figure 43). Therefore it may be concluded that substitution of Cu^{2+} ion ($S = 1/2$) for Ni^{2+} ion ($S = 1$) does not induce AF transition in $PbNi_2V_2O_8$ [114].

Then the next problem is the impurity substitution other than $S = 1/2$. The heat capacity of $Pb(Ni_{1-x}Co_x)_2V_2O_8$ (Co^{2+} ion has $S = 3/2$ spin) was measured in [114] and it is shown in figure 43 [114]. It clearly shows the existence of the ordered phase at 4.3 K, which is higher than the highest transition temperature in $Pb(Ni_{1-x}Mg_x)_2V_2O_8$.

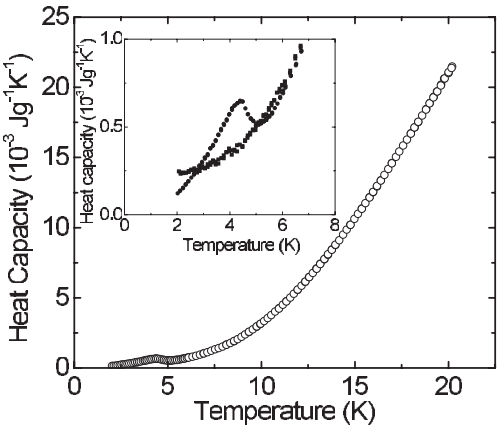

Figure 43. Heat capacity of $Pb(Ni_{0.980}Co_{0.020})_2V_2O_8$ (empty circles and filled circles (in the inset)) and $Pb(Ni_{0.960}Cu_{0.040})_2V_2O_8$ (filled squares in the inset) (reprinted from [114]).

These results indicate that in $PbNi_2V_2O_8$ the impurity-induced ordered phase strongly depends on the S values of the impurity ions substituted for $S = 1$ Ni^{2+} ions. In particular, the absence of the transition in $Pb(Ni_{1-x}Cu_x)_2V_2O_8$ is in sharp contrast to the case of $CuGeO_3$.

5.3. Other impurity-induced ordered phases in low-dimensional spin-gap systems

$SrCu_2O_3$ is another compound with a spin gap, into which the impurities induce an AF phase. It is a typical $S = 1/2$ two-leg ladder system [115] with a spin gap, which was derived from susceptibility [116], $1/T_1$ of Cu NMR [117, 118] and inelastic neutron scattering [119].

Substitution of Zn^{2+} ions for Cu^{2+} ions induces the AF phase, which was found by Azuma *et al* [92] by the measurements of the susceptibility and specific heat. Figure 44 [92] shows the susceptibility versus magnetic field in $Sr(Cu_{1-x}Zn_x)_2O_3$, which clearly shows an anomaly similar to those of $Cu_{1-x}Mg_xGeO_3$ and $Pb(Ni_{1-x}Mg_x)_2V_2O_8$. The existence of AF order was confirmed by NMR studies of [120] for $Sr(Cu_{1-x}M_x)_2O_3$ (M = Zn or Ni) and of [121] for $Sr(Cu_{1-x}Zn_x)_2O_3$ and studied by μSR [122] for $Sr(Cu_{1-x}Zn_x)_2O_3$.

An inelastic neutron scattering study was performed for $Sr(Cu_{1-x}Zn_x)_2O_3$ ($x < 0.04$) [119]. The magnitude of the spin gap was found to be 33 meV independent of x, while the scattering intensity decreases with increasing x. In this respect AFLRO and the spin-gap excitation coexist in $SrCu_2O_3$ at least in the low-concentration region, as was observed in $CuGeO_3$ and $PbNi_2V_2O_8$. To the author's knowledge there has been no report of the inter-chain interaction, probably due to the lack of a large single crystal.

6. Summary

In contrast to the belief that the one-dimensional spin-gap system is robust to external perturbation, the impurity-induced AF phase in low-dimensional spin-gap systems was first observed in $CuGeO_3$. This phenomenon itself was quite a new one, which had no similar example. The AF phase was not a conventional AF state and in the low-concentration region the coexistence of the AFLRO and the dimerization (SP order parameter) was observed. However the phase diagram of impurity-induced AF phases turned out to be more complex than expected. There are two AF phases: the DAF phase in the low-concentration region and the UAF phase

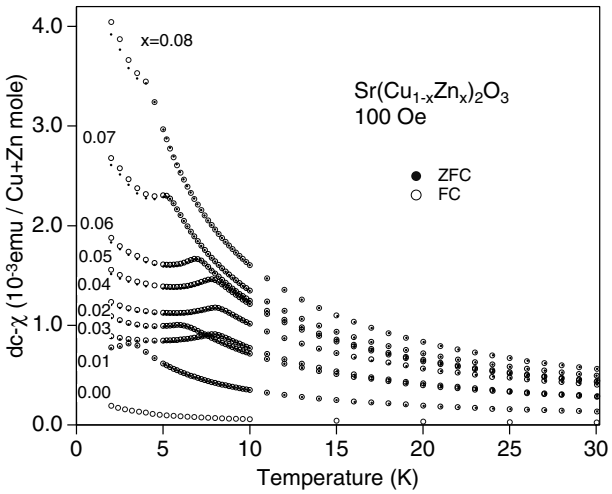

Figure 44. The temperature dependence of the dc magnetic susceptibility of $Sr(Cu_{1-x}Zn_x)_2O_3$ measured in an external field of 100 Oe on heating (closed circles) and cooling (open circles).

in the high-concentration region. This phase transition has been studied by almost all the possible methods by many researchers. The phase diagram and the detailed properties have been investigated.

The physics of pure and impurity-doped $CuGeO_3$ has been providing new phenomena since the discovery [5] of the SP transition in 1993; as was shown in sections 2 and 3 there are still many unsolved problems and the study of this compound will be continued further.

The most important problem is whether the impurity-induced AF phase transition in spin-gap systems is universal or unique to the spin-$\frac{1}{2}$ linear spin system. We have recently found a new Haldane-gap system $PbNi_2V_2O_8$ and also discovered the occurrence of the impurity-induced AF phase in this material [77]. $CuGeO_3$ and $PbNi_2V_2O_8$ have a common property that the inter-chain exchange interaction is relatively strong. What we have found can be explained as follows. It is possible for spin-gap systems with either $S = 1/2$ or 1 spins to have the impurity-induced AF phase(s) if they have relatively strong inter-chain interaction.

More detailed studies are needed to fully understand the impurity-induced phenomena in one-dimensional spin-gap systems, especially, the similarity and the difference between the $S = 1/2$ and 1 systems.

Acknowledgments

The works by the author's group have been performed in cooperation with many people, without whose collaboration the research project would not have developed so widely. I would like to express thanks to all of them.

This research project in the University of Tokyo was partly supported by a Grant-in-Aid for Scientific Research (A), by a Grant-in-Aid for Scientific Research on Priority Area 'Anomalous metallic states near the Mott transition' and by a Grant-in-Aid for COE Research 'Phase control of spin-charge-photon (SCP) coupled systems' from the Ministry of Education, Science, Sports and Culture, Japan, and a NEDO (New Energy and Industrial Technology Development Organization) International Joint Research Grant. The neutron scattering experiments were performed partly through the US–Japan Cooperative Program on Neutron Scattering between USDOE and the Ministry of Education, Science, Sports and Culture, Japan. The author

acknowledges the authors and the publishers for permission to reprint figures: the American Physical Society for figures 1–3, 6–17, 22, 23, 26–31, 34–40 and 44, the Physical Society of Japan for figures 4, 5, 19, 21, 24, 25 and 32 and Elsevier Science for figures 18, 20, 33 and 41–43.

References

[1] Bray J W, Hart H R Jr, Interrante L V, Jacobs I S, Kasper J S, Watkins G D, Wee S H and Bonner J C 1975 *Phys. Rev. Lett.* **35** 744
[2] For a review, see
Bray J W, Interrante L V, Jacobs I S and Bonner J C 1983 *Extended Linear Compounds* vol 3, ed J C Miller (New York: Plenum) p 353
[3] Haldane F D M 1983 *Phys. Lett.* A **93** 464
Haldane F D M 1983 *Phys. Rev. Lett.* **50** 1153
[4] Bednorz J G and Müller K A 1986 *Z. Phys.* B **64** 189
[5] Hase M, Terasaki I and Uchinokura K 1993 *Phys. Rev. Lett.* **70** 3651
[6] Hase M, Terasaki I, Uchinokura K, Tokunaga M, Miura N and Obara H 1993 *Phys. Rev.* B **48** 9616
[7] Hase M, Terasaki I, Sasago Y, Uchinokura K and Obara H 1993 *Phys. Rev. Lett.* **71** 4059
[8] Völlenkle H, Wittmann A and Nowotny H 1967 *Monatsh. Chem.* **98** 1352
[9] Goodenough J B 1955 *Phys. Rev.* **100** 564
Kanamori J 1959 *J. Phys. Chem.* **10** 87
Anderson P W 1963 *Solid State Phys.* **14** 99
[10] Bonner J C and Fisher M E 1964 *Phys. Rev.* **135** A640
[11] Bulaevskii L N 1969 *Fiz. Tverd. Tela.* **11** 1132 (Engl. transl. 1969 *Sov. Phys.–Solid State* **11** 921)
[12] Bulaevskii L N, Buzdin A I and Khomskii D I 1978 *Solid State Commun.* **27** 5
[13] Cross M C 1979 *Phys. Rev.* B **20** 4606
[14] Lorenzo J E, Hirota K, Shirane G, Tranquada J M, Hase M, Uchinokura K, Kojima H, Tanaka I and Shibuya Y 1994 *Phys. Rev.* B **50** 1278
[15] Castilla G, Chakravarty S and Emery V J 1995 *Phys. Rev. Lett.* **75** 1823
[16] Riera J and Dobry A 1995 *Phys. Rev.* B **51** 16 098
[17] Okamoto K and Nomura K 1993 *J. Phys. A: Math. Gen.* **169** 433
[18] Majumdar C K and Ghosh D K 1969 *J. Math. Phys.* **10** 1388
[19] Nishi M, Fujita O and Akimitsu J 1994 *Phys. Rev.* B **50** 6508
[20] For example; Regnault L P, Aïn M, Hennion B, Dhalenne G and Revcolevschi A 1996 *Phys. Rev.* B **53** 5579
[21] Arai M, Fujita M, Motokawa M, Akimitsu J and Bennington S M 1996 *Phys. Rev. Lett.* **77** 3649
[22] Kuroe H, Sekine T, Hase M, Sasago Y, Uchinokura K, Kojima H, Tanaka I and Shibuya Y 1994 *Phys. Rev.* B **50** 16 468
[23] Sekine T, Kuroe H, Sasaki J, Sasago Y, Koide N, Uchinokura K and Hase M 1998 *J. Phys. Soc. Japan* **67** 1440
[24] Kikuchi J, Yasuoka, Hase M, Sasago Y and Uchinokura K 1994 *J. Phys. Soc. Japan* **63** 872
[25] Kamimura O, Terauchi M, Tanaka M, Fujita O and Akimitsu J 1994 *J. Phys. Soc. Japan* **63** 2467
[26] Hirota K, Cox D E, Lorenzo J E, Shirane G, Tranquada J M, Hase M, Uchinokura K, Kojima K, Shibuya Y and Tanaka I 1994 *Phys. Rev. Lett.* **73** 736
[27] Pouget J P, Regnault L P, Ain M, Hennion B, Renard J P, Veillet P, Dhalenne G and Revcolevschi A 1994 *Phys. Rev. Lett.* **72** 4037
[28] Popova M N, Sushkov A B, Golubchik S A, Vasil'ev A N and Leonyuk L I 1998 *Phys. Rev.* B **57** 5040
[29] Damascelli A, van der Marel D, Parmigiani F, Dhalenne G and Revcolevschi A 1997 *Phys. Rev.* B **56** R11 373
[30] Nojiri H, Shimamoto Y, Miura N, Hase M, Uchinokura K, Kojima H, Tanaka I and Shibuya Y 1995 *Phys. Rev.* B **52** 12 749
[31] Griffiths R B 1994 *Phys. Rev.* **133** A768
[32] Ohta H, Imagawa S, Ushiroyama H, Motokawa M, Fujita O and Akimitsu J 1994 *J. Phys. Soc. Japan* **63** 2870
[33] Bloch D, Voiron J, Bonner J C, Bray J W, Jacobs I S and Interrante L V 1980 *Phys. Rev. Lett.* **44** 294
[34] Northby J A, Groenendijk H A, de Jongh L J, Bonner J C, Jacobs I S and Interrante L V 1982 *Phys. Rev.* B **25** 3215
[35] Bloch D, Voiron J, Bray J W, Jacobs I S, Bonner J C and Kommandeur J 1981 *Phys. Lett.* A **82** 21
[36] Cross M C 1979 *Phys. Rev.* B **20** 4606
[37] Nakano T and Fukuyama H 1980 *J. Phys. Soc. Japan* **49** 1679
[38] Nakano T and Fukuyama H 1981 *J. Phys. Soc. Japan* **50** 2489

[39] Fujita M and Machida K 1984 *J. Phys. Soc. Japan* **53** 4395
[40] Hamamoto T, Adachi N, Kido G, Hase M, Sasago Y and Uchinokura K 1994 *J. Phys. Soc. Japan* **63** 1218
[41] Kiryukhin V, Keimer B and Moncton D E 1995 *Phys. Rev. Lett.* **74** 1669
[42] Kiryukhin V and Keimer B 1995 *Phys. Rev.* B **52** R704
[43] Kiryukhin V, Keimer B, Hill J P and Vigliante A 1996 *Phys. Rev. Lett.* **76** 4608
[44] Kiryukhin V, Keimer B, Hill J P, Coad S M and Paul D McK 1996 *Phys. Rev.* B **54** 7269
[45] Fagot-Revurat Y, Horvatić M, Berthier C, Boucher J P, Ségransan P, Dhalenne G and Revcolevschi A 1997 *Phys. Rev.* B **55** 2964
[46] Horvatić M, Fagot-Revurat Y, Berthier C, Dhalenne G and Revcolevschi A 1999 *Phys. Rev. Lett.* **83** 420
[47] Rønnow H M, Enderle M, McMorrow D F, Regnault L-P, Dhalenne G, Revcolevschi A, Hoser A, Prokes K, Vorderwisch P and Schneider H 2000 *Phys. Rev. Lett.* **84** 4469
[48] Zang J, Chakravarty S and Bishop A R 1997 *Phys. Rev.* B **55** R14705
[49] Buzdin A I, Kulic M L and Tugushev V V 1983 *Solid State Commun.* **48** 483
[50] Uhrig G S, Schonfeld F and Boucher J P 1998 *Europhys. Lett.* **41** 431
[51] Takehana K, Takamasu T, Hase M, Kido G and Uchinokura K 2000 *Phys. Rev.* B **51** 5191
[52] Loa I, Gronemeyer S, Thomsen C and Kremer R K 1997 *Z. Phys. Chem.* **201** 333
[53] Lorenz T, Büchner B, van Loosdrecht P H M, Schönfeld F, Chouteau G, Revcolevschi A and Dhalenne G 1998 *Phys. Rev. Lett.* **81** 148
[54] Takehana K, Takamasu T, Hase M, Kido G and Uchinokura K 1998 *Physica* B **246–7** 246
[55] van Loosdrecht P H M, Huant S and Martinez G 1996 *Phys. Rev.* B **54** R3730
[56] Brill T M, Boucher J P, Voiron J, Dhalenne G, Revcolevschi A and Renard J P 1994 *Phys. Rev. Lett.* **73** 1545
[57] Hori H, Furusawa M, Sugai S, Honda M, Takeuchi T and Kindo K 1995 *Physica* B **211** 180
[58] Ando Y, Takeya J, Sisson D L, Doettinger S G, Tanaka I, Feigerson R S and Kapitulnik A 1998 *Phys. Rev.* B **58** R2913
[59] Oseroff S B, Cheong S W, Aktas B, Hundley M F, Fisk Z and Rupp L W Jr 1995 *Phys. Rev. Lett.* **74** 1450
[60] Hase M, Koide N, Manabe K, Sasago Y, Uchinokura K and Sawa A 1995 *Physica* B **215** 164
[61] Hase M, Uchinokura K, Birgeneau R J, Hirota K and Shirane G 1996 *J. Phys. Soc. Japan* **65** 1392
[62] Lussier J-G, Coad S M, McMorrow D F and Paul D McK 1995 *J. Phys.: Condens. Matter* **7** L325
[63] Koide N, Sasago Y, Masuda T and Uchinokura K 1996 *Czech. J. Phys.* **46** (S2) 1981
[64] Koide N, Uchiyama Y, Hayashi H, Masuda T, Sasago Y, Uchinokura K, Manabe K and Ishimoto H 1998 *Preprint* cond-mat/9805095
[65] Hase M, Terasaki I, Sasago Y, Uchinokura K, Tokunaga M, Miura N, Kido G, Hamamoto T and Obara H 1994 *Physica* B **201** 167
[66] Uchinokura K, Hase M and Sasago Y 1995 *Physica* B **211** 175
[67] Hase M, Sasago Y, Terasaki I, Uchinokura K, Kido G and Hamamoto T 1996 *J. Phys. Soc. Japan* **65** 273
[68] Renard J P, Dang K Le, Veillet P, Dhalenne G, Revcolevschi A and Regnault L-P 1995 *Europhys. Lett.* **30** 475
[69] Regnault L P, Renard J P, Dhalenne G and Revcolevschi A 1995 *Europhys. Lett.* **32** 579
[70] Sasago Y, Koide N, Uchinokura K, Martin M C, Hase M, Hirota K and Shirane G 1996 *Phys. Rev.* B **54** R6835
[71] Martin M C, Hase M, Hirota K, Shirane G, Sasago Y, Koide N and Uchinokura K 1997 *Phys. Rev.* B **56** 3173
[72] Coad S, Petrenko O, Paul D McK, Fåk B, Lussier J-G and McMorrow D F 1997 *Physica* B **239** 350
[73] Fukuyama H, Tanimoto T and Saito M 1996 *J. Phys. Soc. Japan* **65** 1182
[74] Kojima K M *et al* 1997 *Phys. Rev. Lett.* **79** 503
[75] Masuda T, Fujioka A, Uchiyama Y, Tsukada I and Uchinokura K 1998 *Phys. Rev. Lett.* **80** 4566
[76] Manabe K, Ishimoto H, Koide N, Sasago Y and Uchinokura K 1998 *Phys. Rev.* B **58** R575
[77] Uchiyama Y, Sasago Y, Tsukada I, Uchinokura K, Zheludev A, Hayashi T, Miura N and Böni P 1999 *Phys. Rev. Lett.* **83** 632
[78] Nakao H, Nishi M, Fujii Y, Hirota K, Masuda T, Uchinokura K and Shirane G 1998 *Meeting Abstracts of the Physical Society of Japan* vol 53 p 472
[79] Nakao H, Nishi M, Fujii Y, Masuda T, Tsukada I, Uchinokura K, Hirota K and Shirane G 1999 *J. Phys. Chem. Solids* **60** 1117
[80] Nakao H, Nishi M, Fujii Y, Masuda T, Tsukada I, Uchinokura K, Hirota K and Shirane G 1999 *J. Phys. Soc. Japan* **69** 3186
[81] Nishi M, Nakao H, Fujii Y, Masuda T, Uchinokura K and Shirane G 2000 *J. Phys. Soc. Japan* **69** 3186
[82] Wang Y J, Kiryukhin V, Birgeneau R J, Masuda T, Tsukada I and Uchinokura K 1999 *Phys. Rev. Lett.* **83** 1676
[83] Masuda T, Tsukada I, Uchinokura K, Wang Y, Kiryukhin V and Birgeneau R J 2000 *Phys. Rev.* B **61** 4103
[84] Kiryukhin V, Wang Y J, LaMarra S C, Birgeneau R J, Masuda T, Tsukada I and Uchinokura K 2000 *Phys. Rev.* B **61** 9527
[85] Takeya J, Tsukada I, Ando Y, Masuda T and Uchinokura K 2000 *Phys. Rev.* B **61** 14 700

[86] According to Fisher's theory antiferromagnetic transition temperatures are determined by the maxima (or a maximum) of $\partial(\chi_c T)/\partial T$ as T_{N1} (lower one) and T_{N2} (higher one) (or T_N, when a single cusp exists). See Fisher M E 1962 *Phil. Mag.* **7** 1731
[87] Harris Q J, Feng Q, Birgeneau R J, Hirota K, Shirane G, Hase M and Uchinokura K 1995 *Phys. Rev.* B **52** 15 420
[88] Masuda T *et al* 2000 *Physica* B **284–288** 1637
[89] Masuda T and Uchinokura K, in preparation
See also Masuda T and Uchinokura K 1999 *Meeting Abstracts of the Physical Society of Japan* vol 54 p 433
[90] Masuda T, Kuroda R and Uchinokura K 2001 *J. Magn. Magn. Mater.* **226–230** 425
[91] Masuda T *et al* 2001 submitted
[92] Azuma M, Fujishiro Y, Takano M, Nohara M and Takagi H 1997 *Phys. Rev.* B **55** R8658
[93] Wichmann R and Müller-Buschbaum Hk 1986 *Rev. Chim. Miner.* **23** 1
[94] Uchiyama Y 1999 *Master Thesis* Department of Applied Physics, The University of Tokyo
[95] Zheludev A, Masuda T, Tsukada I, Uchiyama Y, Uchinokura K, Böni P and Lee S-H 2000 *Phys. Rev.* B **62** 8921
[96] Golinelli O, Jolicœur Th and Lacaze R 1993 *J. Phys.: Condens. Matter* **5** 7847
[97] Gadet V, Verdaguer M, Briois V, Gleizes A, Renard J P, Beauvillain P, Chappert C, Goto T, Dang K Le and Veillet P 1991 *Phys. Rev.* B **44** 705
[98] Zheludev A, Masuda T, Uchinokura K and Nagler S E 2001 *Phys. Rev.* B **64** 134415
[99] Sorensen E S and Affleck I 1994 *Phys. Rev.* B **49** 15 771
[100] Sakai T and Takahashi M 1990 *Phys. Rev.* B **42** 4537
[101] Morra R M, Buyers W J L, Armstrong R L and Hirakawa K 1988 *Phys. Rev.* B **38** 543
[102] Xu G, DiTusa J F, Ito T, Oka K, Takagi H, Broholm C and Aeppli G 1996 *Phys. Rev.* B **54** R6827
[103] Regnault L P, Zaliznyak I, Renard J P and Vettier C 1994 *Phys. Rev.* B **50** 9174
[104] Mutka H, Payen C, Molinié P, Soubeyroux J L, Colombet P and Tayler A D 1991 *Phys. Rev. Lett.* **67** 497
[105] Affleck I, Kennedy T, Lieb E H and Tasaki H 1987 *Phys. Rev. Lett.* **59** 899
Affleck I, Kennedy T, Lieb E H and Tasaki H 1988 *Commun. Math. Phys.* **115** 477
[106] Miyashita S and Yamamoto S 1993 *J. Phys. Soc. Japan* **62** 1459
[107] Hagiwara M, Katsumata K, Affleck I, Halperin B I and Renard J P 1990 *Phys. Rev. Lett.* **65** 3181
[108] Uchinokura K, Uchiyama Y, Masuda T, Sasago Y, Tsukada I, Zheludev A, Hayashi T, Miura N and Böni P 2000 *Physica* B **284–288** 1641
[109] Shender E F and Kivelson S A 1991 *Phys. Rev. Lett.* **66** 2384
[110] Buyers W J L, Morra R M, Armstrong R L, Hogan M J, Gerlach P and Hirakawa K 1986 *Phys. Rev. Lett.* **56** 371
[111] Morra R M, Buyers W J L, Armstrong R L and Hirakawa K 1988 *Phys. Rev.* B **38** 543
[112] Kakurai K, Steiner M, Kjems J K, Petitgrand D, Pynn R and Hirakawa K 1988 *J. Physique Coll.* **49** C8 1433
[113] Sosin S S, Zaliznyak I A, Prozorova L A, Tsipenyuk Yu M and Petrov S V 1997 *J. Exp. Theor. Phys.* **85** 114
[114] Uchinokura K, Masuda T, Uchiyama Y and Kuroda R 2001 *J. Magn. Magn. Mater.* **226** 431
[115] Hiroi Z, Azuma M, Takano M and Bando Y 1991 *J. Solid State Chem.* **95** 230
[116] Azuma M, Hiroi Z, Takano M, Ishida K and Kitaoka Y 1994 *Phys. Rev. Lett.* **73** 3463
[117] Ishida K, Kitaoka Y, Asayama K, Azuma M, Hiroi Z and Takano M 1994 *J. Phys. Soc. Japan* **63** 3222
[118] Ishida K, Kitaoka Y, Tokushige Y, Matsumoto S, Asayama K, Azuma M, Hiroi Z and Takano M 1996 *Phys. Rev.* B **53** 2827
[119] Azuma M, Takano M and Eccleston R 1998 *J. Phys. Soc. Japan* **67** 740
[120] Ohsugi S, Tokunaga Y, Ishida K, Kitaoka T, Azuma M, Fujishiro Y and Takano M 1999 *Phys. Rev.* B **60** 4181
[121] Fujiwara N, Saito T, Azuma M and Takano M 2000 *Phys. Rev.* B **61** 12 196
[122] Larkin M *et al* 2000 *Physica* B **289/290** 153